Developing Chlorin/Arylaminoquinazoline Conjugates with Nanomolar Activity for Targeted Photodynamic Therapy: Design, Synthesis, SAR, and Biological Evaluation

Lubov V. Krylova[a⊥], Vasilii F. Otvagin[a⊥], Galina P. Gribova[a], Natalia S. Kuzmina[a], Ekaterina A. Fedotova[a], Ivan V. Zelepukin[b], Alexander V. Nyuchev[a], Irina V. Balalaeva[a*], Alexey Yu. Fedorov[a*]*

[a]Lobachevsky State University of Nizhny Novgorod, Gagarina av. 23, Nizhny Novgorod 603950, Russian Federation, Fax: +7 831-462-32-32

[b]Shemyakin-Ovchinnikov Institute of Bioorganic Chemistry of the Russian Academy of Sciences, Moscow 117997, Russia

*Corresponding authors.

E-mail addresses: votvagin@yandex.ru (V.F. Otvagin), irin-b@mail.ru (I.V. Balalaeva), afedorovnn@yandex.ru (A.Yu. Fedorov).

1. Introduction

Photodynamic therapy (PDT) is a clinically approved approach for treating cancers and various non-oncological diseases[1]. Generally, PDT relies on the ability of particular photosensitizers (PSs) to generate reactive oxygen species (ROS) under specific light wavelengths. Since the activation of the PS occurs only in areas exposed to light, surrounding healthy tissues are spared from damage, minimizing side effects compared to traditional treatments like chemotherapy or radiation therapy. Notably, PDT outcomes include the induction of an antitumor immune response, giving rise to photodynamic immunotherapy — a promising avenue in anticancer treatments[2].

Despite its positive aspects, application of traditional PSs encounters several drawbacks[3]. These challenges include non-selective PS uptake by tumor tissues, resulting in undesired side effects like prolonged skin and eye phototoxicity, as well as photoallergic reactions. To address these issues and enhance the accumulation of PSs in tumors, active[4] targeting concept has been widely employed. Active targeting strategy centers around molecular recognition of different ligands by receptors overexpressed on the surface of cancer cells[4]. In the ongoing efforts to achieve this, versatile biomacromolecules, including antibodies[4], aptamers[5], nanobodies[6], affibodies[7], and

https://doi.org/10.26434/chemrxiv-2024-qsdbb **ORCID:** https://orcid.org/0000-0001-6015-099X Content not peer-reviewed by ChemRxiv. **License:** CC BY-NC-ND 4.0

peptides[8], have been utilized to create covalent conjugates for PDT (the third generation of PDT agents[9]).

Despite their exceptional affinity to tumor receptors, working with biomacromolecules poses challenges, and the workflow is not always straightforward. In addition, these type ligands are prone to degradation in biological environment via enzymatic cleavage[10]. Linking photosensitizers with small-molecule ligands that are specifically recognized by cancer cell receptors offers an alternative approach to boost selectivity[11,12]. As of now, small-molecule ligands have been derived from tyrosine kinase inhibitors (TKIs) Vandetanib[13–15], Cabozantinib[16], Erlotinib[17–21], Gefitinib[22], Neratinib[23], Lenvatinib[24] and Ganetespib[25]. Such ligands demonstrate a high stability in various experimental conditions bringing numerous synthetic advantages over biomolecules in targeted PDT. Moreover, they can serve a dual role by both targeting and inhibiting proteins of interest[12].

Among the plethora of receptors involved in tumor cell progression, a special focus is placed on EGFR (epidermal growth factor receptor)[26]. Over last decades many successful studies on EGFR-targeted PSs have been published, where targeting EGFR was achieved through binding to its intracellular or extracellular domain. In fact, in the last case biomolecules or peptides are routinely applied, while intracellular domain can be reached using small molecule ligands[27]. Despite the fact that the intracellular domain of EGFR is not readily exposed on a cell's surface, various researchers have reported improved selectivity for PSs conjugated with small EGFR inhibitors[14,19,22,23].

Our research group has recently suggested several multifunctional PSs for targeting delivery and combinational therapy purposes[13,14,16]. Among molecules evaluated, conjugate **1**[14], consisted of a chlorin-e_6 photosensitizer and a Vandetanib derivate, exhibited the pronounced selectivity toward EGFR-expressing tumor cells (Figure 1). Vandetanib **2** belongs to TKIs and was approved in 2011 for the treatment of late-stage medullary thyroid cancer[28]. Its mechanism of action includes blocking the activity of EGFR and VEGFR thereby hindering signal transduction in tumor cells.

Chlorin-e_6 derivatives represent a convenient platform for creating new photosensitizers. As derivatives of chlorophyll-*a* with absorption occurring within a phototherapeutic window (> 650

https://doi.org/10.26434/chemrxiv-2024-qsdbb **ORCID:** https://orcid.org/0000-0001-6015-099X Content not peer-reviewed by ChemRxiv. **License:** CC BY-NC-ND 4.0

nm), these PDT agents enable efficient ROS generation and rapid excretion from the patient's body[29]. However, many photosensitizers, including chlorin-e_6 derivatives, are recognized for their limited solubility in water solutions, which significantly hampers their photodynamic potential[30]. To overcome this issue, we introduced quaternary ammonium salts into the structure of **1**. Quaternary ammonium cations provide required hydrophilicity for PSs and are well-known for their favorable impact on photodynamic activity[31–33].

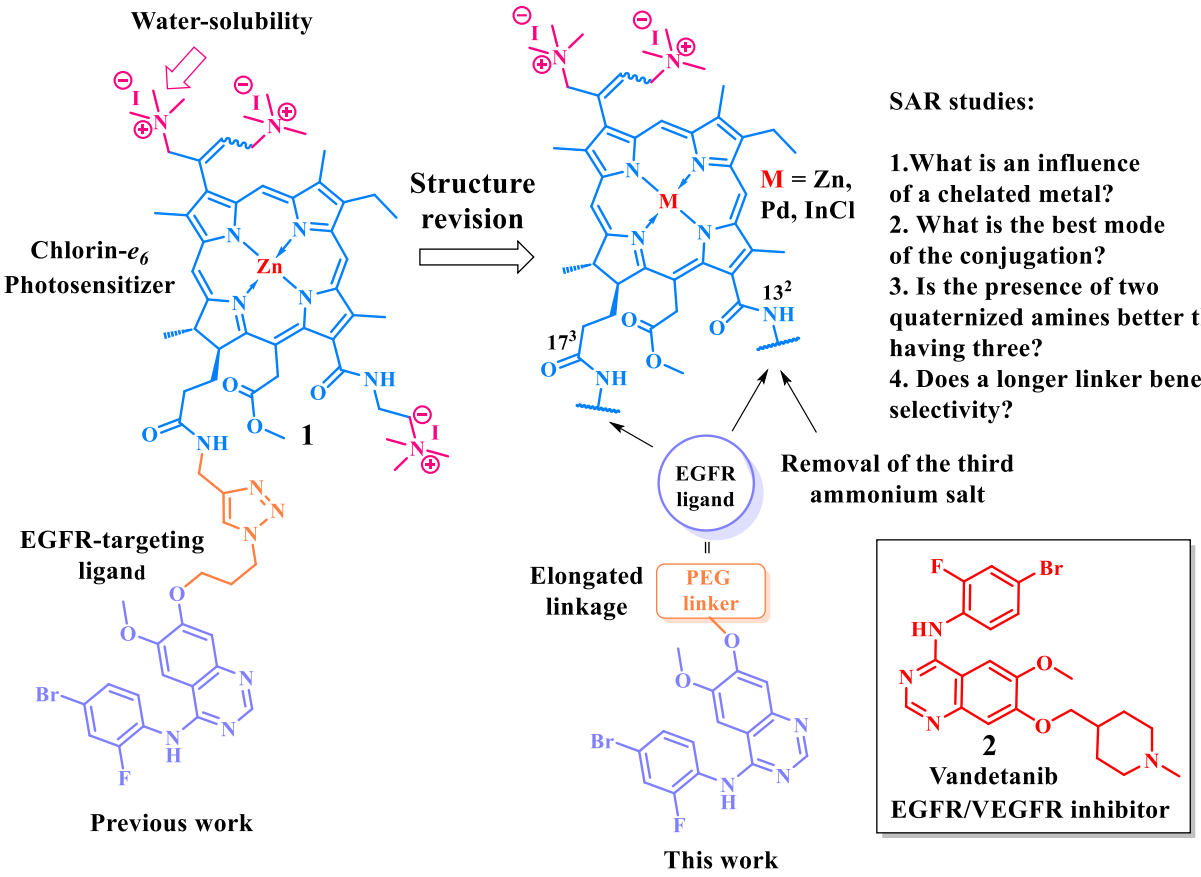

Figure 1. Structures of EGFR-targeted conjugates and Vandetanib.

Inspired by the findings, we decided to further explore this concept and conduct SAR studies for conjugate **1**. In this work we aim to assess how structural features, namely, a conjugation pattern, choice of a complexed metal and number of positive charges, might influence selectivity and photodynamic activity of such conjugates.

As it was demonstrated by Pandey et al, a ligand's attachment position may alter EGFR targeting properties for conjugate of HPPH photosensitizer (pyropheophorbide-*a* derivative) with Erlotinib (EGFR inhibitor)[20]. To enhance the population of the triplet state through the heavy atom effect

https://doi.org/10.26434/chemrxiv-2024-qsdbb ORCID: https://orcid.org/0000-0001-6015-099X Content not peer-reviewed by ChemRxiv. License: CC BY-NC-ND 4.0

(HAE), different chlorin-e_6 metallocomplexes have been synthesized and characterized[34]. Notably, Pd- and In-complexes have garnered considerable attention[35]. Consequently, we applied the same techniques to enhance the photodynamic activity of our EGFR-targeted conjugates in this study.

The introduction of cationic moieties is beneficial for solubility of PSs and can ensure additional organelle-targeting properties[33]. However, an excessive amount of positively charged groups makes a PS highly hydrophilic hampering its internalization through the cellular membrane. Generally, mono- or dicationic photosensitizers exhibit best performance, readily passing through the lipid bilayer[32]. Charge symmetry is another important factor worth considering. For instance, Araki and Baptista proposed that dicationic photosensitizers with a one-sided charge distribution should be optimal for successful internalization[36]. Building upon these findings, we decided to remove the cationic moiety at the 13^2 position in conjugate **1** to prepare dicationic conjugates.

To make the conjugates more flexible and reduce the steric hindrance with EGFR, we replaced the short ether linker with the longer PEG-type linker.

Herein, we report the SAR studies of the chlorin-e_6 photosensitizers conjugated with the Vandetanib derivative. The antitumor performance and selectivity of these novel PDT agents are evaluated both *in vitro* and *in vivo*.

2. Results and discussion

2.1.Chemistry

First, we performed a computational docking analysis to predict whether a PEG-substituted vandetanib derivative **3** could still maintain its binding to ATP-binding site of EGFR (Fig. 2(A, B)). The results suggested that the conformations of Vandetanib **2** (cornflower blue) and **3** (pink) are well matched, and that the PEG linker of **3** is sufficiently exposed toward surface of the EGFR. Importantly, the vandetanib derivative **3** were found to preserve the conventional hydrogen bond with MET769 – a key residue in the binding of EGFR inhibitors with quinazoline scaffolds[37].

https://doi.org/10.26434/chemrxiv-2024-qsdbb **ORCID:** https://orcid.org/0000-0001-6015-099X Content not peer-reviewed by ChemRxiv. **License:** CC BY-NC-ND 4.0

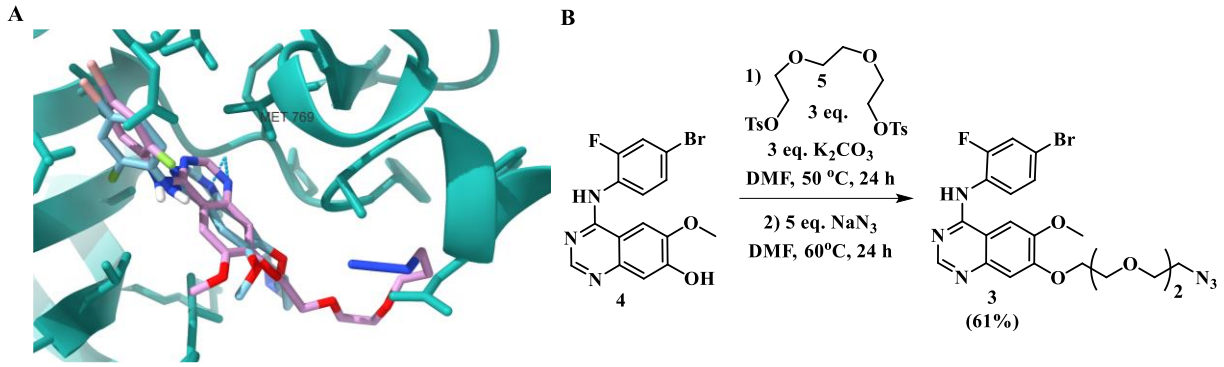

Figure 2. (A) Modeled conformations of vandetanib **2** (pink) and its derivative **3** bound to EGFR (PDB: 1M17). (B) Synthesis of **3**.

After establishing that compound **3** could function as an EGFR-targeting ligand, we proceeded with its synthesis, starting from the previously obtained vandetanib derivative **4**[14] with an available phenolic position (Fig. 2(B)). Compound **3** was furnished after two steps that included alkylation with ditosylate **5** followed by azidation.

Then, the azide-containing compound **3** was subjected to Cu (I)-catalyzed azide-alkyne cycloaddition (CuAAC) with the propargyl-substituted chlorin **6** leading to the conjugate **7** in a 79% yield (Scheme 1). The chlorin **6** was synthesized according to our previous report[14]. To introduce additional dimethylaminomethyl groups, we employed the double aminomethylation transformation of the vinylic position in chlorins in the presence of *N,N,N′,N′*-tetramethyldiaminomethane[38,39]. This reaction allowed us to obtain the aminomethylated conjugate **8** with an 65% yield as a mixture of inseparable isomers. Finally, the quaternization reaction with CH_3I yielded the desired tricationic photosensitizer **9** with a quantitative yield.

Scheme 1. Synthesis of the tricationic conjugate **9**.

https://doi.org/10.26434/chemrxiv-2024-qsdbb **ORCID:** https://orcid.org/0000-0001-6015-099X Content not peer-reviewed by ChemRxiv. **License:** CC BY-NC-ND 4.0

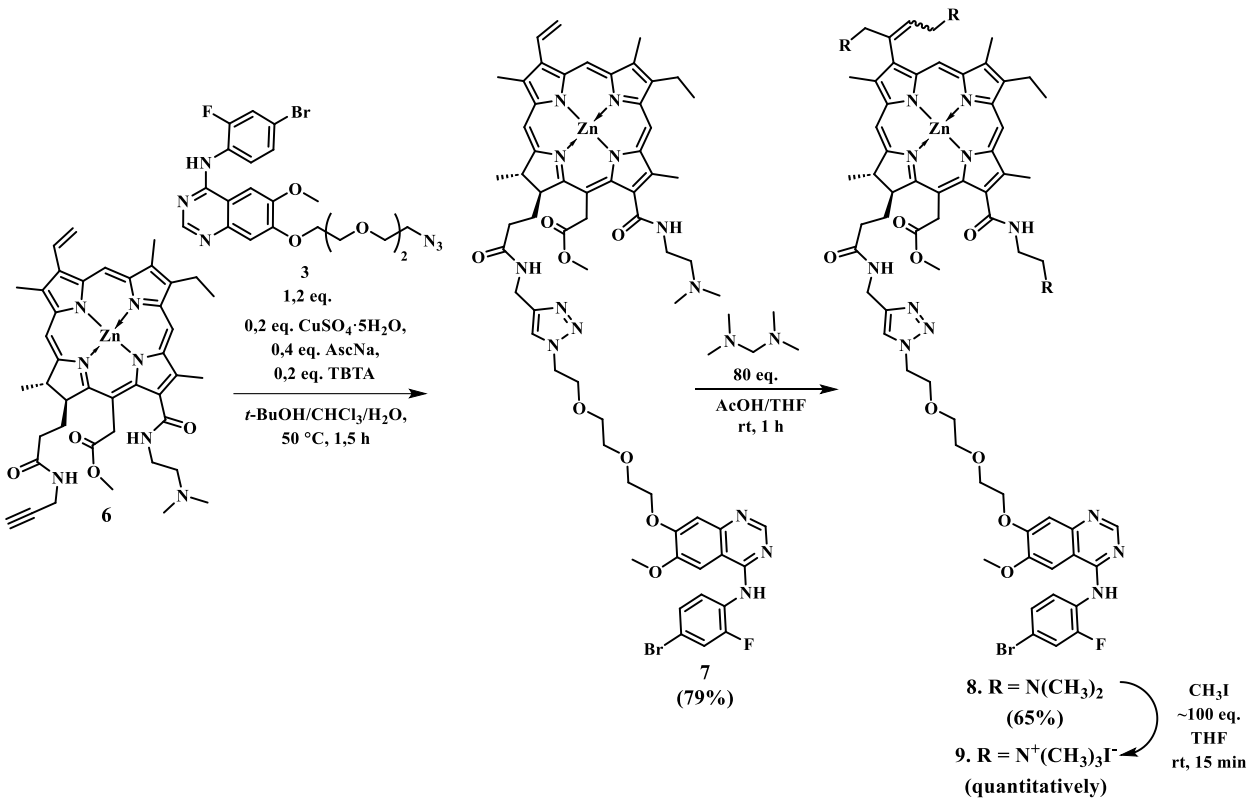

To obtain dicationic conjugates, we performed a nucleophilic ring-opening of the five-membered exocycle in methylpheophorbide-*a* (MePheid-*a*) **10** with propargyl amine followed by complexation with zinc (Scheme 2). The yield of the resulting zinc-containing chlorin **11** was 89% after two steps. Its subsequent conjugation with **3** under CuAAC conditions gave conjugate **12** with a 79% yield. Utilizing the aminomethylation-quaternization strategy, we synthesized desired dicationic conjugate **14** with an altered mode of conjugation between active parts.

Scheme 2. Synthesis of the dicationic conjugate **14**.

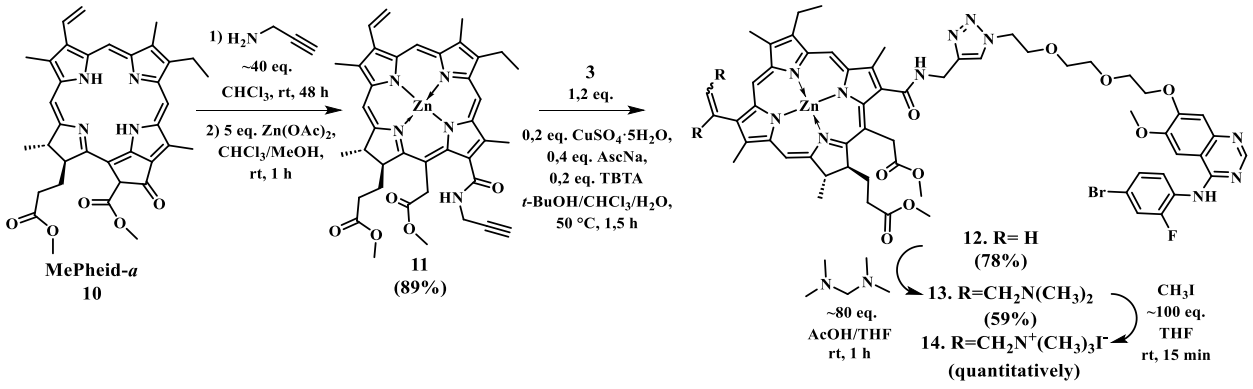

Our further efforts focused on synthesizing of dicationic conjugates containing In- and Pd-metallocomplexes of chlorins (Scheme 3). Given that zinc can be easily removed from a chlorin

https://doi.org/10.26434/chemrxiv-2024-qsdbb ORCID: https://orcid.org/0000-0001-6015-099X Content not peer-reviewed by ChemRxiv. License: CC BY-NC-ND 4.0

core, we demetallated conjugate **13** in the presence of TFA. Both steps yielded In-complex **15** with a 56% yield. It should be noted that due to axial Cl atom, In-complex **15** represents a mixture of diasteromers[40]. Again, quaternization with CH_3I was applied to furnish dicationic conjugate **16** in a quantitative yield. However, the same strategy proved unsuccessful for the Pd-complex, as treatment with $Pd(OAc)_2$ led to the decomposition of the demetallated intermediate.

Scheme 3. Synthesis of the dicationic conjugate **16**.

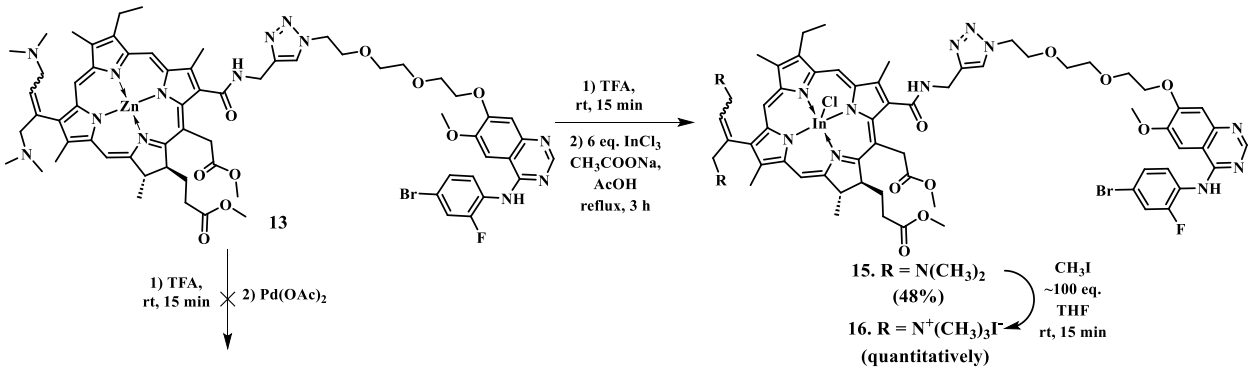

Following the synthetic scheme, developed for Zn-containing dicationic conjugate **14**, we faced challenges in introducing Pd into the chlorin core due to potential interference with the propargyl moiety. However, by adopting a reported reaction involving MePheid-*a* **10** and $Pd(OAc)_2$ in MeCN[41], we successfully obtained its Pd-complex, which was subsequently transformed into the alkyne-containing chlorin derivative **18** (Scheme 4). Finally, conjugation with **3**, followed by the aminomethylation-quaternization sequence, led to the desired dicationic Pd-complex **20**.

Scheme 4. Synthesis of the dicationic conjugate **20**.

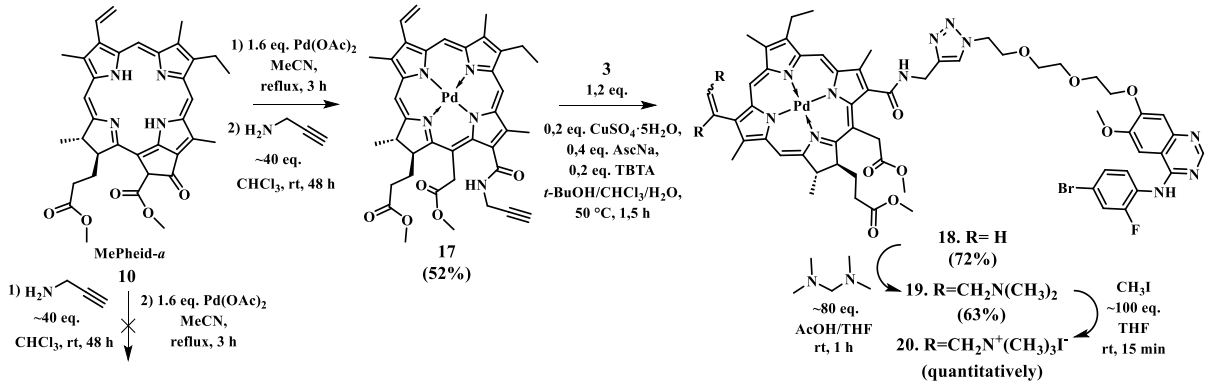

Once required conjugates **9, 14, 16** and **20** were obtained, we proceeded with the synthesis of reference chlorin photosensitizers lacking EGFR-targeting moiety (Scheme 5). These compounds

https://doi.org/10.26434/chemrxiv-2024-qsdbb **ORCID:** https://orcid.org/0000-0001-6015-099X Content not peer-reviewed by ChemRxiv. **License:** CC BY-NC-ND 4.0

served as a necessary control group in biological assays. To mimic the linker in the conjugates, we employed 1-(2-azidoethoxy)-2-(2-methoxyethoxy)ethane **21,** which underwent a high-yielding CuAAC reaction with **11**. The resulting chlorin **22** was then aminomethylated, yielding chlorin **23** with an 85% yield. Subsequent quaternization of **23** with CH_3I led to Zn-containing reference dicationic photosensitizer **24**. Acidic demetallation of **23**, followed by refluxing with $InCl_3$, was utilized to synthesize In-complex **25**. In the last step, amino groups in **25** was transformed into ammonium salts via reaction with CH_3I. Due to unsatisfactory photophysical parameters of dicationic Pd-conjugate **20** and tricationic Zn-conjugate **9** (discussed below), it was decided not to prepare reference chlorins of similar structures.

Scheme 5. Synthesis of the reference chlorins **24** and **26**.

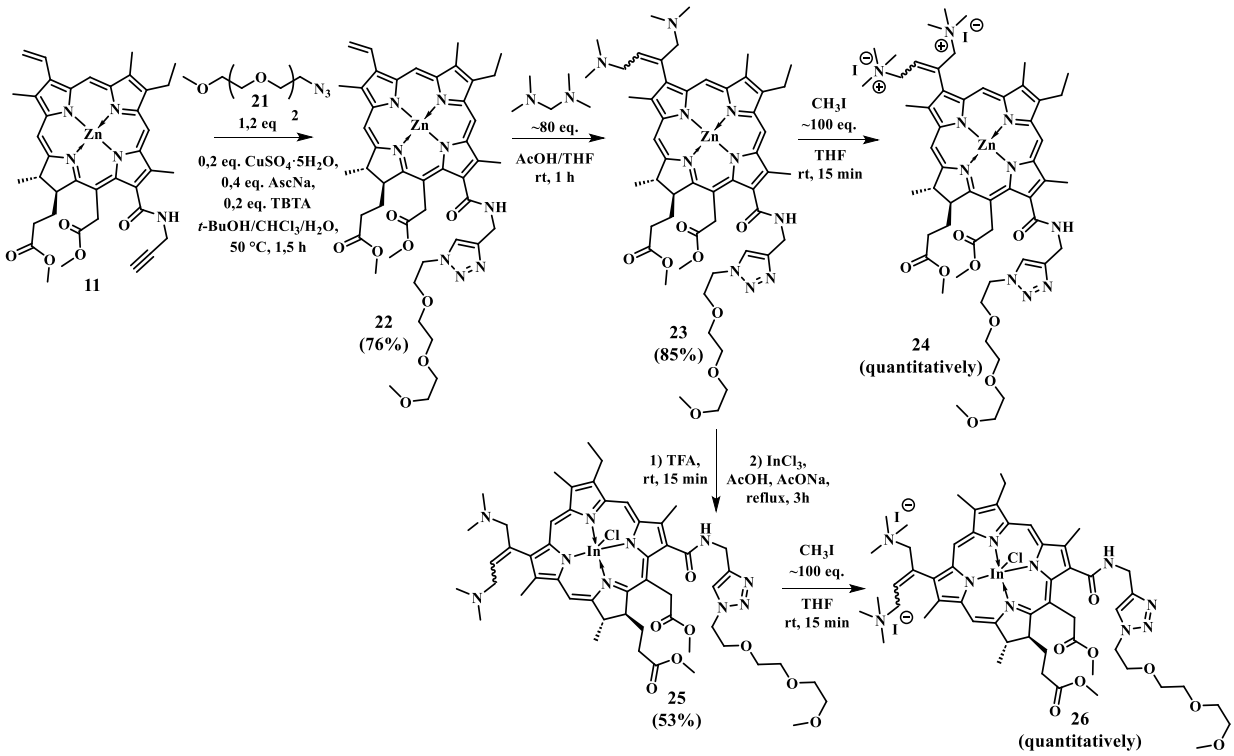

Overall, the proposed synthetic routes allowed us to synthesize one conjugate **9 (Zn-3)** bearing three charges; three conjugates **14 (Zn-2), 16 (In-2)** and **20 (Pd-2)** all bearing two charges. Additionally, we obtained two reference chlorins without the EGFR-ligand and bearing two charges: **24 (r-Zn-2)** and **16 (r-In-2)**. Due to the presence of positively charged moieties, all photosensitizers demonstrated sufficient solubility and formed homogeneous solutions in PBS (up to ~1mM concentrations). However, time-dependent precipitation was observed in some of these

https://doi.org/10.26434/chemrxiv-2024-qsdbb **ORCID:** https://orcid.org/0000-0001-6015-099X Content not peer-reviewed by ChemRxiv. **License:** CC BY-NC-ND 4.0

solutions, which prompted us to use non-toxic additives to stabilize them in biological tests (for details, see Experimental Part).

2.2.Photophysical properties

Having synthesized the set of conjugated photosensitizers along with unconjugated analogs, we set out to explore their properties under light irradiation. The conjugates **9 (Zn-3), 14 (Zn-2), 16 (In-2)** and **20 (Pd-2)** demonstrated typical absorption spectra (Fig. 3(A)) for chlorin derivatives (Soret and Q bands). As expected, the insertion of metals influenced electronic transition in the conjugates and reference chlorins. A slight bathochromic shift was observed for **16 (In-2)** in comparison with **9 (Zn-3)** and **14 (Zn-2)**, while **20 (Pd-2)** exhibited a hypsochromic shifting. Chlorins **24 (r-Zn-2)** and **16 (r-In-2)** followed the same pattern (Figure S56). Among all tested compounds, the **20 (Pd-2)** conjugate had the weakest Q-band, which was in accordance with literature precedents[42]. Clearly visible absorption around 350 nm for all PSs indicated the presence of the Vandetanib moiety.

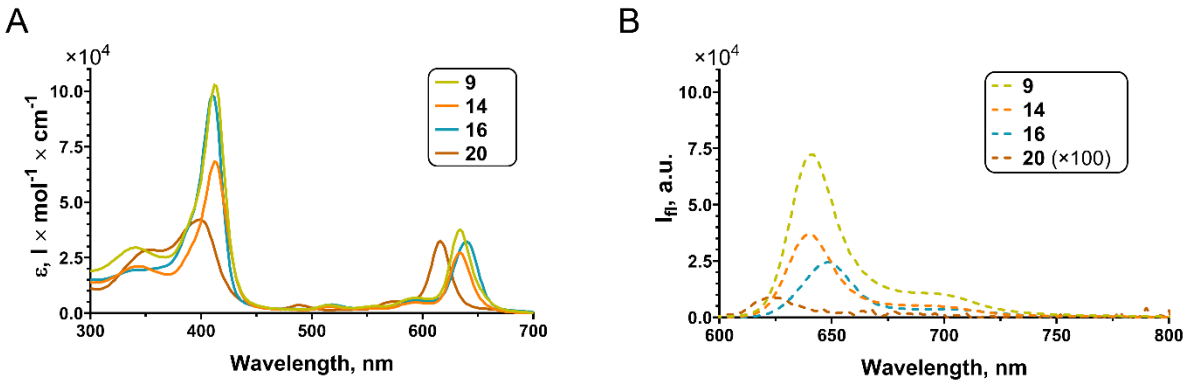

Figure 3. (A) UV-Vis absorption and (B) fluorescence (λ_{ex} = 410 nm) spectra of the conjugates **9 (Zn-3), 14 (Zn-2), 16 (In-2)** and **20 (Pd-2)** (5 μM) in water.

Upon excitation at 410 nm, conjugates **14 (Zn-2)** and **16 (In-2)** exhibited fluorescence (Fig. 2(B)) with a fluorescence quantum yield (Φ_F) of ~1.5% (Table 1). In contrast, the fluorescence signal recorder for tricationic conjugate **9 (Zn-3)** was a 3-times stronger with Φ_F of 6%. As dicationic chlorin **24 (r-Zn-2)** showed strong fluorescence (Φ_F = 10%), we believe that the number of positive charges didn't affect the emission spectra. However, a pronounced difference in

https://doi.org/10.26434/chemrxiv-2024-qsdbb **ORCID:** https://orcid.org/0000-0001-6015-099X Content not peer-reviewed by ChemRxiv. **License:** CC BY-NC-ND 4.0

fluorescence quantum yield for dicationic Zn-complexes **14 (Zn-2)** and **24 (r-Zn-2)** suggested that the Vandetanib moiety acted as a quencher for **14 (Zn-2)**. Interestingly, the photophysical behavior of In-complexes **16 (In-2)** and **26 (r-In-2)** was not affected by the attachment of the Vandetanib counterpart. We speculate that the axial ligand in In-conjugate **16 (In-2)** prevented π-π stacking with the quinazoline core, otherwise quenching emission in **14 (Zn-2)**. Due to weak emission, we could not record fluorescence spectra and calculate Φ_F for Pd-complex **20 (Pd-2)**. This result was also consistent with literature examples where Pd-pheophorbide complexes had Φ_F ~0.01%[42].

Table 1. Photophysical characterization of the synthesized chlorins.

Compound	λ_{abs} (nm) / log ε	λ_{em}[a] (nm)	Φ_F[b] (%)	Φ_Δ[c] (%)
9	412 / 5	642	6.0	29 (DMSO)
	634 / 4.6			2.8 (PBS)
14	412 / 4.8	640	1.7	19 (DMSO)
	634 / 4.4			8.9 (PBS)
16	410 / 5	648	1.2	51 (DMSO)
	640 / 4.5			43.1 (PBS)
20	400 / 4.6	-	-	19 (DMSO)
	616 / 4.5			16 (PBS)
24	408 / 4.9	638	10	28.4 (DMSO)
	630 / 4.4			3.4 (PBS)
26	406 / 4.7	644	1.6	53.8 (DMSO)
	634 / 4.3			29.6 (PBS)

[a]Excited at 410 nm. [b]Relative to Rhodamine B in water. [c]Determined using 1,3-diphenylisobenzofuran (DPBF) and anthracene-9,10-diylbis-methylmalonate (ADMA) as chemical traps (relative to Photoditazine®).

The assessment of singlet oxygen (SO) generation quantum yield (Φ_Δ) was conducted using SO-sensitive chemical traps (Table 1). The high efficiency of SO generation is crucial for successful photodynamic therapy (PDT) and can vary significantly for a particular photosensitizer depending

https://doi.org/10.26434/chemrxiv-2024-qsdbb **ORCID:** https://orcid.org/0000-0001-6015-099X Content not peer-reviewed by ChemRxiv. **License:** CC BY-NC-ND 4.0

on the chemical surroundings. Therefore, we employed 1,3-diphenylisobenzofuran trap (DPBF) for DMSO solutions and anthracene-9,10-diylbis-methylmalonate trap (ADMA) to study SO generation in PBS solutions. The solution of Photoditazine® in DMSO or in PBS was used as a standard (for details, see Experimental Part).

All photosensitizers generated SO in DMSO with Φ_Δ of ~19-54%, while their SO generation ability was reduced in PBS with Φ_Δ of ~3-43%. In the case of the conjugates **16 (In-2)** and **20 (Pd-2)**, this result was clearly due to the lifetime of SO decreasing in water environments. However, other compounds, particularly Zn-complexes **9 (Zn-3), 14 (Zn-2)** and **24 (r-Zn-2)**, demonstrated significantly dropped Φ_Δ values in PBS, which could not be explained by this hypothesis. The observed pattern could again be evidence of increased intramolecular or intermolecular π-π stacking in the investigated Zn-complexes. Among all photosensitizers, In-substituted derivatives **16 (In-2)** and **26 (r-In-2)** were the most efficient SO generators with Φ_Δ of 30-43% in PBS.

Another important parameter, namely photostability, was determined for conjugates **9 (Zn-3)**, **14 (Zn-2)**, and **16 (In-2)**. As we executed this experiment by monitoring the fluorescence response from conjugates under increasing power of light irradiation, the nonfluorescent conjugate **20 (Pd-2)** was excluded from this assessment. From Figure S57, it can be seen that the In-containing conjugate **16 (In-2)** was sufficiently stable, while the conjugate **14 (Zn-2)** was moderately stable, and the conjugate **9 (Zn-3)** rapidly photobleached. Interestingly, the observed tendency didn't correspond to Φ_Δ values of the conjugates, implying that their photostability was not related to self-oxidation of the conjugates by generating SO. The calculated quantum yield of photobleaching was: 2.6×10^{-9} for **16 (In-2)**, 4.5×10^{-9} for **14 (Zn-2)** and 7.8×10^{-9} for **9 (Zn-3)**.

Obviously, a high SO generation yield along with resistance to photobleaching is desirable for a prospective photosensitizer. Therefore, the conjugate **16 (In-2)**, which had both features, was identified as a promising candidate for further investigation in PDT. The less appealing dicationic Zn-complex **14 (Zn-2)** was also chosen for further biological experiments. The tricationic Zn-complex **9 (Zn-3)** was excluded at this stage due to poor photostability combined with low SO

https://doi.org/10.26434/chemrxiv-2024-qsdbb **ORCID:** https://orcid.org/0000-0001-6015-099X Content not peer-reviewed by ChemRxiv. **License:** CC BY-NC-ND 4.0

generation yield in PBS. Although the Pd-complex **20 (Pd-2)** maintained high Φ_Δ values in PBS, its nonfluorescent nature obstructed its diagnostic utility in PDT through fluorescence imaging. Consequently, conjugate **20 (Pd-2)** was deemed unsuccessful in this context.

2.3.Cellular uptake study

With the optimal photosensitizers in hand, we proceeded to investigation of their ability to penetrate the cell's membrane and be accumulated in the living cells. For this purpose, we applied cancerous and normal cell cultures varying in EGFR expression, namely A431 cells (human epidermoid squamous carcinoma, EGFR positive) and HaCat (human keratinocytes, control). EGFR expression levels are well-documented in the literature for these cells[43] and were verified independently by us[14]. Additionally, cutaneous squamous cell carcinoma (SCC) represents a promising therapeutic target for PDT[44].

At first, we incubated A431 and HaCat cells with **14 (Zn-2)** and **16 (In-2)** and recorded their fluorescence at different time intervals (Figure S58). The fluorescence of the conjugates gradually increased with extended incubation time, reaching its maximum after 24 hours. Consequently, we decided to incubate the conjugates **14 (Zn-2)**, **16 (In-2)** and the reference chlorins **24 (r-Zn-2)**, **26 (In-2)** with the cells for 24 h (Figure 4(A, B)). In this experiment fluorescence signal of all the compounds was detected in the perinuclear region indicating successful uptake by A431 and HaCat cells. Despite higher fluorescence yields, the reference chlorin **24 (r-Zn-2)** demonstrated weaker fluorescence response in cells. In contrast, the conjugate **14 (Zn-2)**, with approximately 5 times lower fluorescence yield, displayed a signal in the cells that was 2-6 times stronger. Likely, the presence of the EGFR-targeting ligand, based on the Vandetanib derivative, facilitated its accumulation. The observed result aligns with our previous study, where tricationic Zn-conjugate **1** (Figure 1) demonstrated similar selectivity toward A431 cell line[14]. Therefore, it can be concluded that Zn-conjugates, bearing two charges, still maintained their targeting potential. A completely different outcome was recorded after a comparison was made between the conjugate **16 (In-2)** and the chlorin **26 (In-2)**. Both the conjugated and unconjugated analogs showed similar

https://doi.org/10.26434/chemrxiv-2024-qsdbb **ORCID:** https://orcid.org/0000-0001-6015-099X Content not peer-reviewed by ChemRxiv. **License:** CC BY-NC-ND 4.0

uptake in the cells, implying that the Vandetanib ligand didn't improve delivery for **16 (In-2)**. Since **16 (In-2)** is formally a tricationic compound, considering the ionic nature of the In-Cl bond, we assume that this structural feature is not favorable for its binding with the intracellular domain of EGFR.

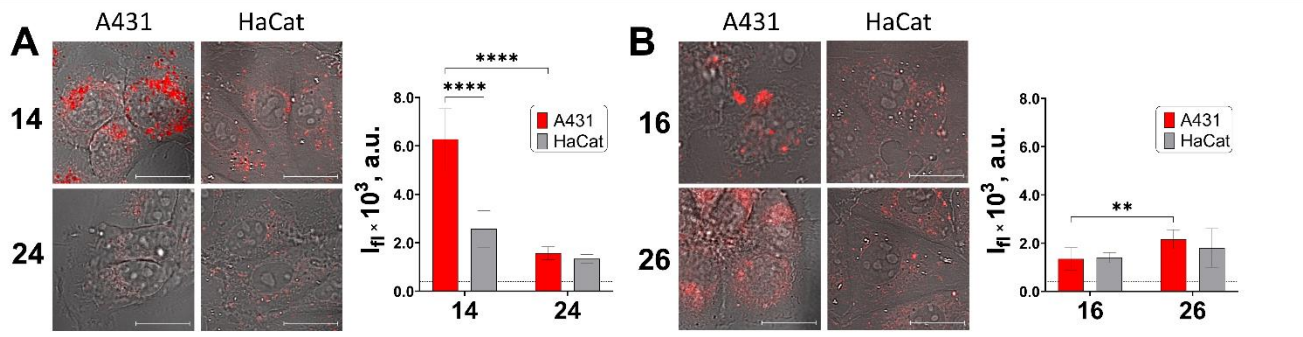

Figure 4. Cellular uptake study of: (A) **14 (Zn-2)** and **24 (r-Zn-2)**; (B) **16 (In-2)** and **26 (r-In-2)**. Confocal images of the living cells after 24 h incubation in the serum-free growth medium containing 5 μM of a tested compound, the merged images in transmitted light and red fluorescence are shown, bar is 20 μm. Results of the qualitative analysis of the cellular fluorescence signal. The level of autofluorescence is represented by a dotted line. At least ten cells in two-three fields of view were analyzed; means ± SD. Statistically significant difference in relative fluorescence (**** - $p < 0.0001$, ** - $p < 0.01$ two-way ANOVA with post hoc test for multiple comparisons).

To gain further insights into the uptake of conjugates by cells, we evaluated their partition coefficients (logP) in *n*-octanol/water mixtures. Among the tested compounds, conjugate **16 (In-2)** was the most lipophilic, with a logP of 0.19. In contrast, conjugate **14 (Zn-2)** was primarily distributed in the water phase, with a calculated logP of -2.47. Although lipophilic substances typically diffuse more readily across cell membranes, conjugate **16 (In-2)** did not demonstrate sufficient absorption by A431 cells compared to the hydrophilic conjugate **14 (Zn-2)**. Therefore, this parameter cannot account for the observed differences in accumulation of the conjugates *in vitro*.

https://doi.org/10.26434/chemrxiv-2024-qsdbb **ORCID:** https://orcid.org/0000-0001-6015-099X Content not peer-reviewed by ChemRxiv. **License:** CC BY-NC-ND 4.0

The co-localization analysis using dyes specific to particular cellular organelles revealed that the conjugates **14 (Zn-2)**, **24 (r-Zn-2)** and the chlorins **16 (In-2)** and **26 (r-In-2)** predominantly localized in lysosomes (Figure 5, Figure S59). This observation led us to hypothesize active ATP-dependent endocytosis for the tested PSs, a mechanism also suggested for the structurally similar chlorin conjugates in our previous studies[18]. It's worth noting that lysosome targeting is a crucial strategy to enhance PDT efficiency[45]. Therefore, the pronounced localization of the conjugates **14 (Zn-2)** and **16 (In-2)** in these vesicles could be highly advantageous. The PDT-induced disintegration of the lysosomal membrane results in the cytoplasmic release of metal ions and hydrolases, triggering cell death through pathways including cathepsin-, calpain-, and calcium-dependent mechanisms[46].

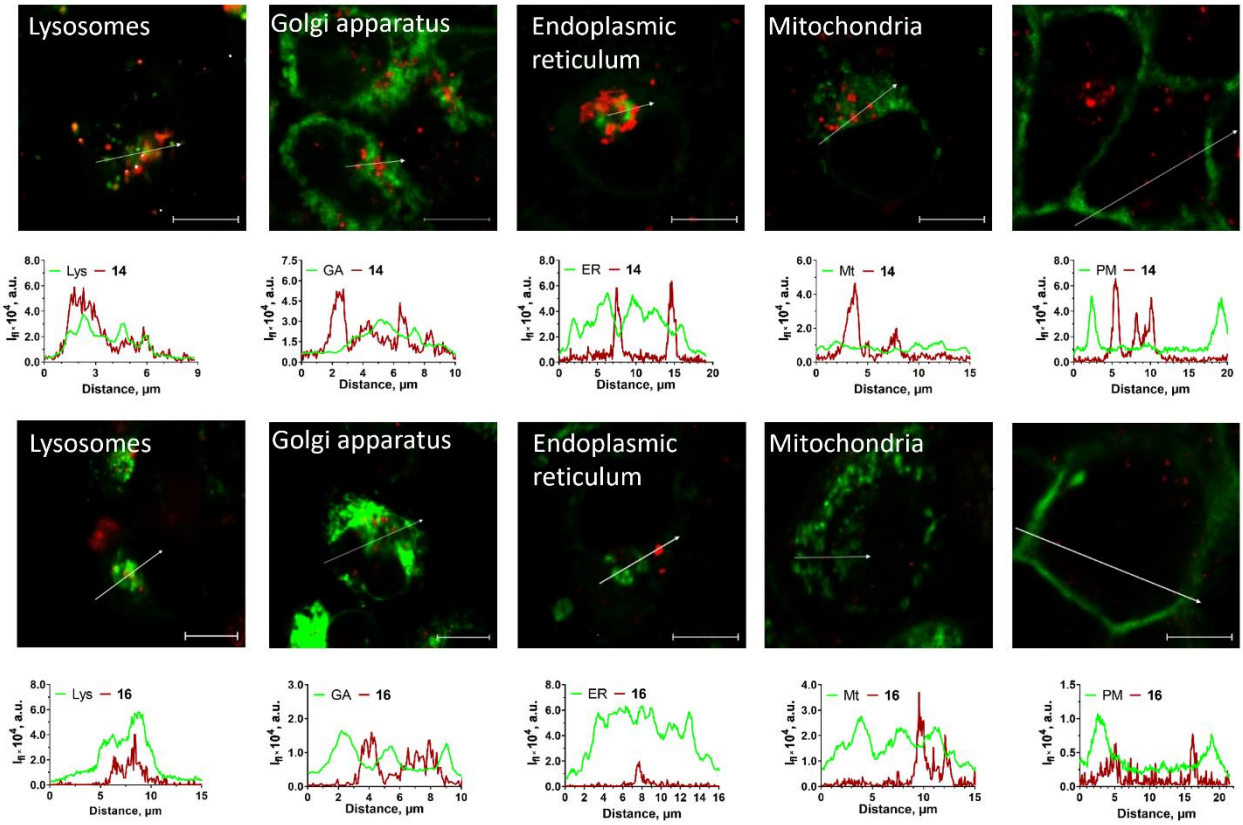

Figure 5. Analysis of intracellular localization of **14** (a) and **16** (b) in A431 cells. The cells were incubated with the compounds (5 μM) for 24 hours and then stained with the following dyes: LysoTracker Green for lysosomes (Lys); MitoTracker Green for mitochondria (Mt); ER-Tracker for ER and BODYPY FL C5-ceramide complexed to BSA for Golgi apparatus (GA); CellMask™ Plasma Membrane Stain for the cell membrane (PM). The merged fluorescent channels for the

https://doi.org/10.26434/chemrxiv-2024-qsdbb **ORCID:** https://orcid.org/0000-0001-6015-099X Content not peer-reviewed by ChemRxiv. **License:** CC BY-NC-ND 4.0

dyes (green) and the compounds (red) are presented; fluorescence signal profiles are shown along the lines indicated by the white arrow on the images. Scale bars, 10 μm.

2.4.Photodynamic Activity in Vitro

To assess the therapeutic performance of the conjugates **14 (Zn-2)** and **16 (In-2)**, at the next step we tested their ability to induce the cell death in *in vitro* cultures of A431 and HaCat cells. The "dark" and photoinduced toxicity was compared to the reference compounds **24 (r-Zn-2)** and **26 (r-In-2).**

Without photodynamic activation, **24 (r-Zn-2)** showed toxicity in concentarions about 100 μM, while its EGFR-targeting analog **14 (Zn-2)** displayed toxicity at significantly lower concentrations (Figure 6 and Table 2). Of importance, half-maximal inhibiting concentration of **14 (Zn-2)** ($IC_{50\ Dark}$) was about 4-fold lower for EGFR-expressing A431 cells (10.3 vs 39.13 μM for HaCat cells). Upon light irradiation at a dose of 20 J/cm^2, the cytotoxicity of both **24 (r-Zn-2)** and **14 (Zn-2)** significantly rose (24-37-fold). The $IC_{50\ Light}$ of **24 (r-Zn-2)** didn't statistically differ between two cell lines; while in case of **14 (Zn-2)**, again, the $IC_{50\ Light}$ value was evidently lower for A431 cells comparing to HaCat (0.28 μM vs. 1.64 μM). We attribute this specificity of **14 (Zn-2)** cytotoxic action to the vandatenib moiety which enhances the conjugate's affinity for A431 cells and blocks the transduction of mitogenic signals through EGFR overexpressed in these cells due to gene amplification.

Similar dependencies were observed for In-containing conjugate **16 (In-2)** and chlorin **26 (r-In-2)**. Without photodynamic activation, the conjugate and its unconjugated analog inhibited cell proliferation at 10-30 μM concentrations. In case of **16 (In-2)**, $IC_{50\ Dark}$ was about 3-fold lower for A431 cells. Both In-substituted compounds expressed higher photodynamic activity than Zn-substituted, with selectivity against A431 cells. The highest photo-induced toxicity, about 9 nM, was registered for **16 (In-2)**. This result underscores the promising photodynamic performance of **16 (In-2)**. To our knowledge, natural-derived PSs rarely remain cytotoxic in this range. Even more appealing is a profound selectivity shown for the conjugate **16 (In-2)**, as it was approximately 30

https://doi.org/10.26434/chemrxiv-2024-qsdbb **ORCID:** https://orcid.org/0000-0001-6015-099X Content not peer-reviewed by ChemRxiv. **License:** CC BY-NC-ND 4.0

times more phototoxic in tumor cells A431 than in HaCat cells. Another important finding was the impressive $IC_{50\ Dark}$ / $IC_{50\ Light}$ ratio calculated to be more than 10^3 for **16 (In-2)**.

We should note that if in case of **14 (Zn-2)** its selectivity was in accordance with its preferential accumulation in A431 cells, the reasons behind exceptional photodynamic activity for **16 (In-2)** remain unclear. One possibility is that the Vandetanib ligand was detached from the conjugates in cells. Following binding of the quinazoline scaffold to its cellular targets might amplify overall antiproliferation effect. As it was demonstrated for Vandetanib **2** alone, its cytotoxic potency was maintained in both cell lines preferably aimed at EGFR-expressing A431 cells. To verify this hypothesis, we subjected cell's lysates, incubated with **14 (Zn-2)** and **16 (In-2)**, to HPLC analysis (see SI). As a result, the liberation of the Vandetanib derivative was not detected. Consequently, other mechanisms should exist for **16 (In-2)** to provide additional combinational synergistic effect. ROS generation ability, being almost identical for **16 (In-2)** and **26 (r-In-2)**, also could not be the case. More studies are underway to clarify how **16 (In-2)** interact with cellular environment.

Table 2. *In vitro* light and dark cytotoxic activity of **3** and **26**.

Compound/ Cell line		**$IC_{50\ Dark}$, μM**	**$IC_{50\ Light}$, μM**	**$IC_{50\ Dark}$/ $IC_{50\ Light}$**
14	**A431**	10.3 [6.8-15.5]*	0.28 [0.16-0.5]*	37
	HaCat	39.13 [34.03-44.98]	1.64 [1.05-2.5]	24
24	**A431**	about 100[#]	1.64 [1.2-2.3]	>61
	HaCat	101.8 [21.18-489.3]	1.63 [1.45-1.8]	>33
16	**A431**	10.76 [5.1-22.67]*	0.009 [0.075-0.012]**	1195
	HaCat	28.84 [26.9-30.88]	0.21 [0.17-0.26]	109
26	**A431**	11.81 [9.4-14.79]**	0.21 [0.09-0.48]	56
	HaCat	12.81 [5.44-30.17]	0.17 [0.13-0.23]	167
2	**A431**	4.3 [2.9-6.2]**	-	-
	HaCat	8.3 [7.2-9.6]		

Statistically significant difference from HaCat cell line in each group (*– $p<0.0001$, ** – $p<0.01$ *t*-test)

[#], the experimental data do not allow calculation of statistically significant value

https://doi.org/10.26434/chemrxiv-2024-qsdbb **ORCID:** https://orcid.org/0000-0001-6015-099X Content not peer-reviewed by ChemRxiv. **License:** CC BY-NC-ND 4.0

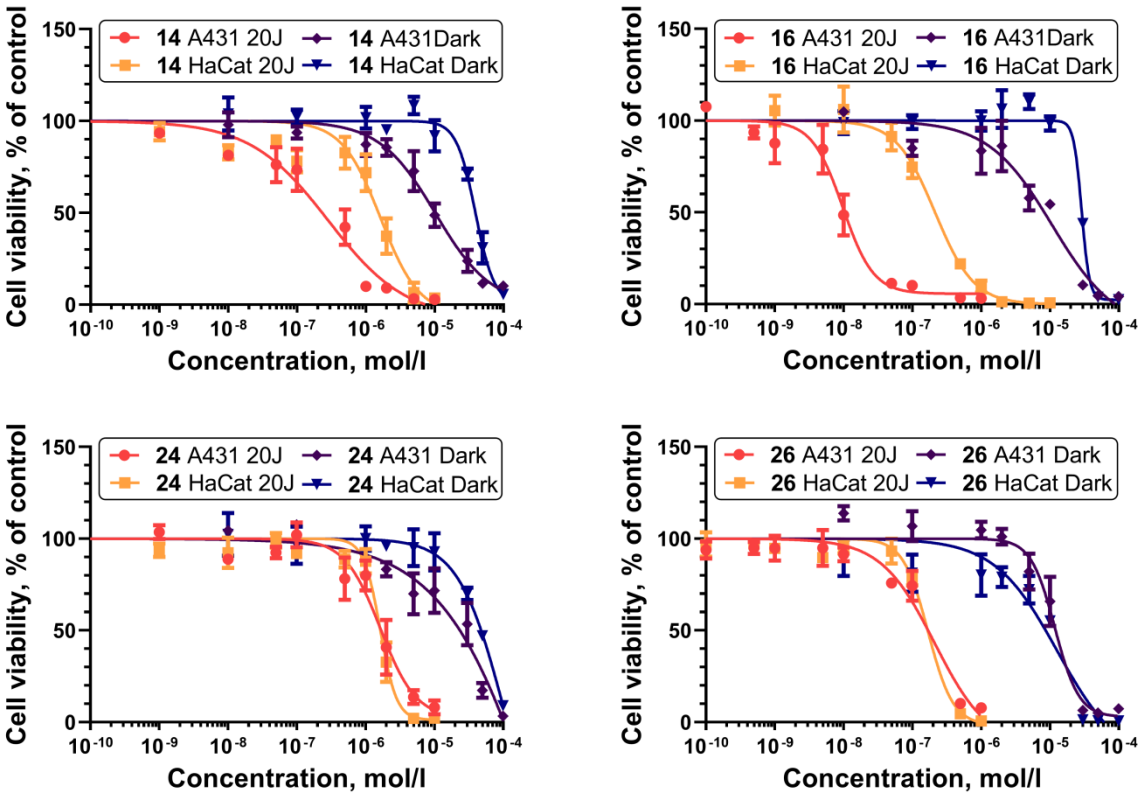

Figure 6. Relative viability of A431 and HaCat cells treated with **14** (a), **16** (b), **24** (c) and **26** (d) with (20 J) or without (Dark) light exposure. Cells were incubated with the tested compounds for 24 h, the medium was exchanged with full fresh growth medium, and the cells were irradiated in dose of 20 J/cm^2 (655-675 nm, 32 mW/cm^2 power) or stayed in dark. After the additional incubation for 24 h, cell viability was measured by MTT-assay and expressed as the percentage to untreated cells. Means ± SD are presented; the experimental data are fitted using four parameters model.

2.5. *In Vivo* Antitumor Potency

Once we confirmed that conjugates **14 (Zn-2)** and **16 (In-2)** induced photodynamic effects in cell cultures, we proceeded to investigate their activity in nude mice bearing A431 xenograft tumors. To assess the biodistribution of the compounds, they were intravenously administered to tumor-bearing animals at a dose of 8 mg/kg. The pharmacokinetic profile of the compounds was studied by fluorometric analysis of blood samples at various time intervals after injection (Fig.

https://doi.org/10.26434/chemrxiv-2024-qsdbb **ORCID:** https://orcid.org/0000-0001-6015-099X Content not peer-reviewed by ChemRxiv. **License:** CC BY-NC-ND 4.0

7A). It was shown that both the compounds are characterized by a fast decline phase, which indicates a rapid entry of the conjugates into the tissues within first 15-30 min. It resulted in a consequent increase in fluorescence detected by surface fluorescence imaging in both tumor and normal tissues (Figure 7 (B, C)). In line with blood concentration dynamics, the rate of normal tissue accumulation was higher for **14 (Zn-2)**; the signal reached maximum in 0.5 h with following rapid clearance. The In-conjugate **16 (In-2)** continued to accumulate in normal tissue until 1 h time point. Both **14 (Zn-2)** and **16 (In-2)** preferentially accumulated in the tumor with time-delay comparing to normal tissue and maximal signal observed 4 h after injection. At this time point, tumor-to-normal tissue ratio was about 1.5. The noticeable feature of **16 (In-2)** was relatively longer retention in normal and especially in tumor tissue. Likely, lipophilic nature of **16 (In-2)** was responsible for the latter observation, as lipophilic drugs are known to be eliminated more slowly from the body.[47]

To verify the *in vivo* results and evaluate the organ distribution of the conjugates, we sacrificed the mice at the point of maximal tumor fluorescence, 4 h after injection, and imaged the organs and tumors *ex vivo* (Fig. 7D). The conjugate **14 (Zn-2)** is characterized by a noticeably higher level of fluorescence signal in all the organs than **16 (In-2)** which is consistent with *in vivo* results and can be explained by the higher fluorescence quantum yield of **14 (Zn-2)**. At the same time, it's worth pointing out the comparable fluorescence signal from the excised tumor and muscle for mice injected with **14 (Zn-2)**. In contrast, the conjugate **16 (In-2)** has a greater visible tumor-to-muscle contrast, which may indicate more efficient accumulation of this conjugate in the tumor.

https://doi.org/10.26434/chemrxiv-2024-qsdbb **ORCID:** https://orcid.org/0000-0001-6015-099X Content not peer-reviewed by ChemRxiv. **License:** CC BY-NC-ND 4.0

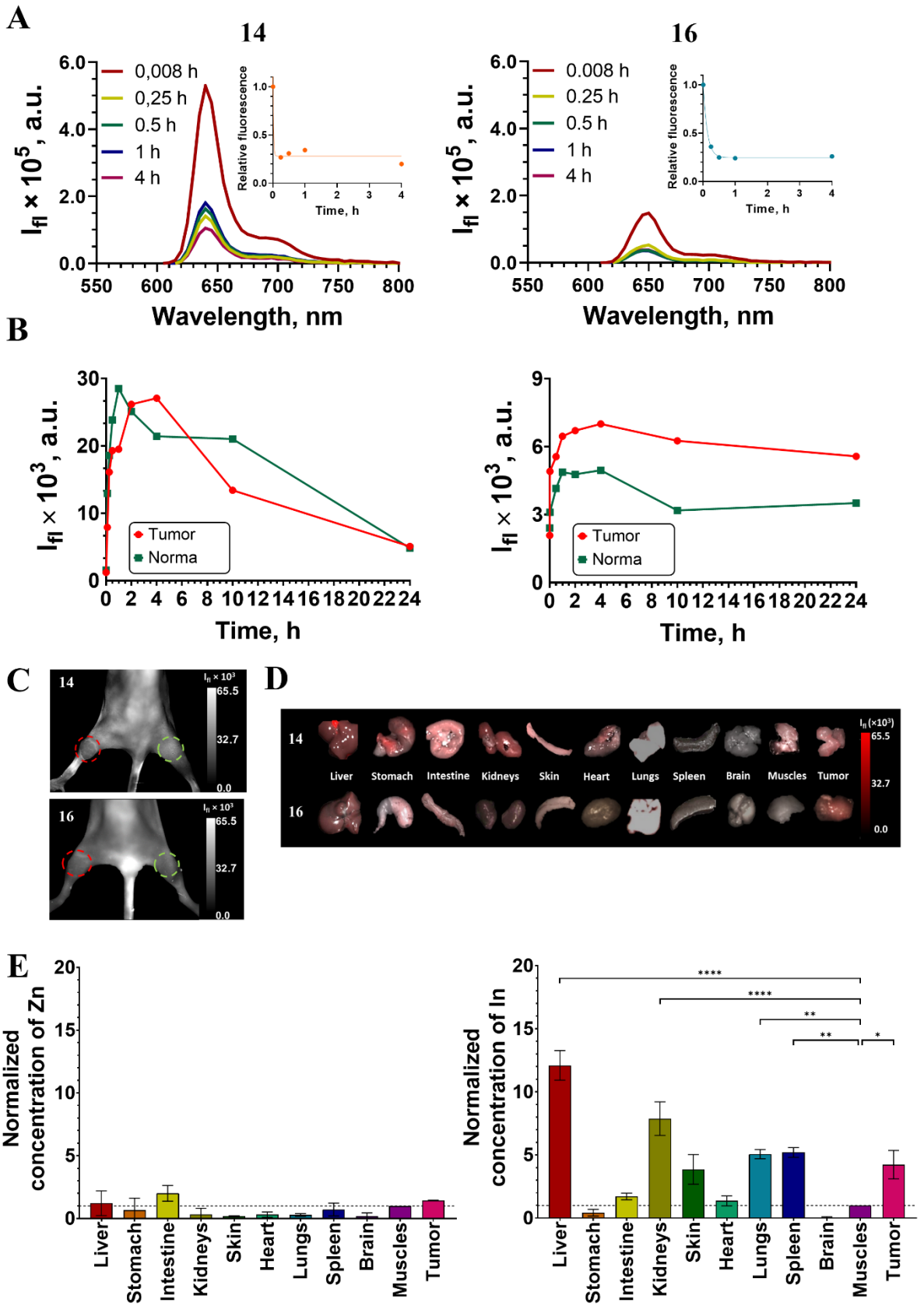

Figure 7. *In vivo* and *ex vivo* biodistribution of **14** and **16**. A) *In vivo* pharmacokinetics of conjugates in mice blood. Emission spectra of blood samples after intravenous injection of **14** and

https://doi.org/10.26434/chemrxiv-2024-qsdbb **ORCID:** https://orcid.org/0000-0001-6015-099X Content not peer-reviewed by ChemRxiv. **License:** CC BY-NC-ND 4.0

16 at different time points, λ_{ex} 410 nm. B) *In vivo* dynamics of the fluorescence intensity in the tumor (red) and normal tissue (green) of animals injected with the conjugates **14 (Zn-2)** and **16 (In-2)**. λ_{ex} 590 nm, λ_{em} 600−700 nm. Representative curves are shown. C) *In vivo* fluorescent images in A-431 tumor-bearing mice at 4 h after intravenous injectionof the conjugates, λ_{ex} 590 nm, λ_{em} 600−700 nm. The tumor is indicated by a dashed red line, normal tissue, a dashed green line. D) *Ex vivo* representative images of organs and tumor. Bright-field and fluorescence images of excised organs and tumors at 24 h after intravenous injection of conjugates are overlayed. λ_{ex} 590 nm, λ_{em} 600−700 nm. E) The elemental analysis of the excised organs and tumors at 4 hours after intravenous administration. Normalized concentration of Zn or In are shown. The concentration of Zn or In in each organ and tumor was normalized to concentration in muscles. The dotted line indicates the normalized metal concentration in the muscle. Statistically significant difference from muscle (**** - $p < 0.0001$, ** - $p < 0.01$, * - $p < 0.05$; two-way ANOVA with post hoc analysis).

The presence of a central metal atom in the tetrapyrrole structure made it possible to quantify the distribution of conjugates in organs and tumors using mass spectrometry. We normalize the Zn and In concentration in every organ to muscle tissue to analyze their relative content. In accordance with the results of *ex vivo* fluorescence analysis, no differential accumulation of **14 (Zn-2)** in tumors was registered. Thus, signal amplification in the tumor was not confirmed. Maximum accumulation in the skin is achieved one hour after intravenous administration of **14 (Zn-2)**, and in the tumor after 2-4 hours with rapid elimination. In contrast, conjugate **16 (In-2)** showed pronounced accumulation in the tumor with tumor-to-muscle ratio of about 3.5. The main organs where **16 (In-2)** accumulated were the liver and kidneys involved in elimination of xenobiotics from the body. Also, the significant accumulation was registered in the lungs and spleen which may be a side effect of the use of PEG as a solvent.[48]

https://doi.org/10.26434/chemrxiv-2024-qsdbb **ORCID:** https://orcid.org/0000-0001-6015-099X Content not peer-reviewed by ChemRxiv. **License:** CC BY-NC-ND 4.0

From the comparison of **14 (Zn-2)** and **16 (In-2)** in *in vitro* and *in vivo* experiments, we conclude that the In-containing derivative **16 (In-2)** exhibits superior characteristics. Its beneficial features include high photostability, activity against tumor cells in nanomolar concentrations, and selective accumulation in tumor. To further prove its therapeutic potential, we performed PDT on A431 tumor-bearing mice with this compound as a photosensitizer. A 0.5 mM solution of **16 (In-2)** was administered to mice via the tail vein at a dose of 8.7 mg/kg. PDT was conducted four hours after intravenous administration using a LED light source (Figure 10(A,B)).

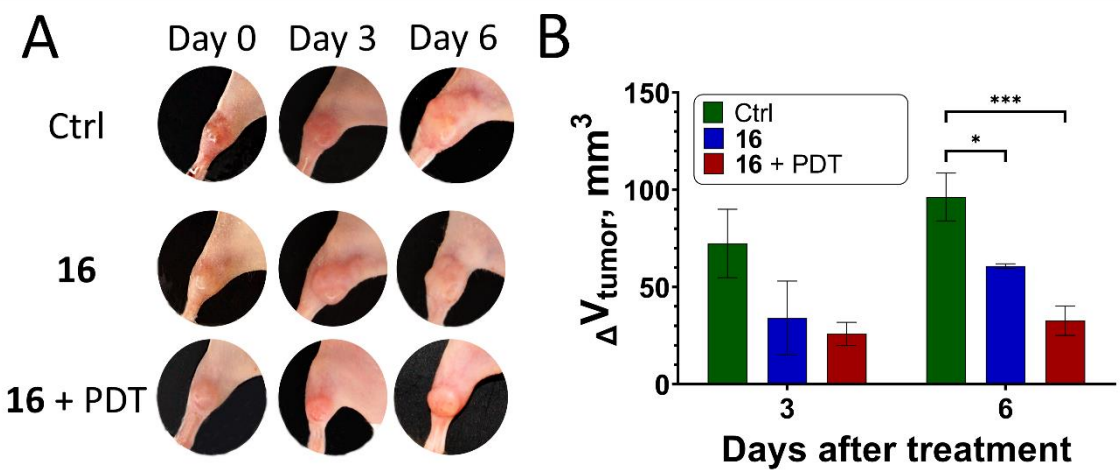

Figure 8. Therapeutic efficacy of **16 (In-2)** against EGFR-positive tumor A431 *in vivo*: A) Representative photographs of tumor in control group without treatment ("**Ctrl**"); tumor in groups with injected conjugate 16 without irradiation ("**16**") and with PDT ("**16+PDT**). B) Change in the volume of tumor nodes of mice in the control and treated groups at days 3 and 6 after treatment. Means ± standard deviation (SD) are presented. The initial mean tumor volume in every group was about 50 mm^3. The growth was measured for individual animals; then, the mean and SD were calculated. Statistically significant difference from the control group (**** - $p < 0.0001$, * - $p < 0.05$; analysis of variance (ANOVA) with Tukey's post hoc test).

PDT treatment led to a significant inhibition of tumor growth. In control group of animals, the size of the tumors increased threefold within six days, from 50 to 150 mm^3 (ΔV_{tumor} of 100 mm^3). In the PDT-treated group, ΔV_{tumor} didn't exceed 25 mm^3; thus, the growth was inhibited by 70 %.

https://doi.org/10.26434/chemrxiv-2024-qsdbb **ORCID:** https://orcid.org/0000-0001-6015-099X Content not peer-reviewed by ChemRxiv. **License:** CC BY-NC-ND 4.0

Interestingly, conjugate **16 (In-2)** demonstrated also moderate therapeutic activity against A431 tumors without light irradiation, with the growth inhibition by 40% (Figure 10(B)). We speculate that this result may be attributed to the inhibition of EGFR by the vandetanib moiety. A similar result was observed for one of our previous chlorin/vandetanib conjugates under similar experimental conditions[13]. In addition, the inhibition of EGFR autophosphorylation was recently reported for erlotinib-platinum(II) photosensitizers[17].

3. Conclusions

In conclusion, we reported the synthesis, SAR studies and biological evaluation of a series of conjugated cationic photosensitizers designed to enhance the selectivity and efficiency of PDT. These conjugates were derived from established chlorin photosensitizers linked to the vandetanib moiety, known for its affinity toward EGFR/VEGFR – proteins overexpressed in tumor tissues. The conjugation of PSs with TKIs is a powerful approach to gain selectivity and obtain synergism during PDT[11,12,49].

To evaluate the impact of metal complexes in the chlorin/vandetanib conjugates, we synthesized a series of molecules incorporating Zn, In, and Pd chlorin metallocomplexes. Although Pd-conjugate **20 (Pd-2)** exhibited high yields of singlet oxygen generation, it proved unsuccessful due to its poor fluorescence, which hinders potential imaging applications. Oppositely, Zn and In complexes **9 (Zn-3)**, **14 (Zn-2)**, and **16 (In-2)** exhibited suitable photophysical parameters. However, tricationic conjugate **9 (Zn-3)** rapidly degraded under light, indicating that this molecule may not be an efficient photosensitizing drug. Notably, the incorporation of the heaviest In atom led to remarkable yields of singlet oxygen generation exceeding 40% even in PBS solutions of **16 (In-2)**.

Two lead compounds, **14 (Zn-2)** and **16 (In-2)**, along with control chlorins **24 (r-Zn-2)** and **26 (r-In-2)**, lacking the vandetanib moiety, were studied *in vitro* using the EGFR-expressing tumorous A431 cell line and the EGFR-negative keratinocytes HaCat as controls. Both conjugates exhibited the ability to inhibit cell proliferation under light, demonstrating selectivity towards

https://doi.org/10.26434/chemrxiv-2024-qsdbb **ORCID:** https://orcid.org/0000-0001-6015-099X Content not peer-reviewed by ChemRxiv. **License:** CC BY-NC-ND 4.0

A431 cells, which could be attributed to the combined action of the vandetanib ligand. Among tested compounds, In-complex **16 (In-2)** exhibited nanomolar activity under light and a remarkable phototoxicity index ($IC_{50\ Dark}$ / $IC_{50\ Light}$) of about 10^3. Accumulation studies showed that compounds **14 (Zn-2)** and **16 (In-2)** readily penetrated the cellular membrane and accumulated in various organelles, primarily lysosomes. Although **16 (In-2)** exhibited comparable levels of fluorescence in both cell lines, **14 (Zn-2)** was preferentially absorbed by A431 cells.

Administration of **16 (In-2)** into mice with implanted A431 tumor xenografts led to its rapid and selective accumulation in tumor with less favorable results for **14 (Zn-2)**. Based on these findings, we performed PDT-treatment using the most promising conjugate, **16 (In-2)**. Preliminary *in vivo* study proved that **16 (In-2)** has the therapeutic potency both without or, to significantly higher extent, under light exposure, highlighting its potential for the development of a therapeutic agent for combination therapy.

4. Experimental section

4.1.General Procedures

^{1}H NMR and ^{13}C NMR spectra were recorded on Agilent DD2 400 MHz spectrometer. Chemical shifts (δ) are reported in ppm for a solution of a compound in $CDCl_3$ or DMSO-d_6, with a residual peak of solvent as an internal reference, *J* values in Hertz. Mass spectra were recorded using: the MALDI method on a time-of-flight Bruker Microflex LT mass-spectrometer. TLC analyses were carried out on Merck TLC Silica gel 60 F254. Column chromatography separation was performed using Macherey-Nagel Kieselgel 60 (70-230 mesh). Purity the targeted compounds was analyzed by high-performance liquid chromatography (HPLC) (Knauer Smartline S2600) using C-18 column (Diasphere 110-C18, Column 250 x 4 mm. All tested compounds were found to be ≥95% pure. Commercially available reagents (Aldrich, Abcr, Alfa Aesar) were used without additional purification. Solvents were purified according to the standard procedures. Petroleum ether (PE) used was of bp 40-70 °C.

4.2.Synthesis and Characterization

https://doi.org/10.26434/chemrxiv-2024-qsdbb **ORCID:** https://orcid.org/0000-0001-6015-099X Content not peer-reviewed by ChemRxiv. **License:** CC BY-NC-ND 4.0

7-(2-(2-(2-azidoethoxy)ethoxy)ethoxy)-N-(4-bromo-2-fluorophenyl)-6-methoxyquinazolin-4-amine (3): The Schlenk flask was charged with quinazolinol derivative **4** (0.330 g, 0.91 mmol), ditosylate **5** (1.25 g, 2.73 mmol), and K_2CO_3 (0.377 g, 2.73 mmol). The system was then purged with argon, and anhydrous DMF (6 mL) was added. The mixture was stirred on a magnetic stirrer for 24 hours at 50 °C. After completion of the reaction (monitored by TLC), the mixture was cooled, and the solvent was evaporated under reduced pressure. The residue was dissolved in $CHCl_3$ (100 mL), washed with H_2O (3 × 50 mL), dried (Na_2SO_4), and concentrated in another Schlenk flask. The flask was then purged with argon, and anhydrous DMF (3 mL) was added, along with NaN_3 (0.295 g, 4.550 mmol). The mixture was stirred for additional 24 hours on a magnetic stirrer at 60 °C. The solvent was then removed under reduced pressure. The residue was dissolved in $CHCl_3$ (100 mL), washed with H_2O (3 × 50 mL), dried (Na_2SO_4), and concentrated again under reduced pressure. The product was purified by column chromatography (EtOAc) to obtain a white solid (0.269 g, 0.555 mmol, 61%). ^{1}H NMR (400 MHz, DMSO-d_6): δ 9.54 (s, 1H), 8.35 (s, 1H), 7.80 (s, 1H), 7.66 (dd, J = 10.0, 2.1 Hz, 1H), 7.53 (t, J = 8.3 Hz, 1H), 7.50 – 7.43 (m, 1H), 7.21 (s, 1H), 4.30 – 4.24 (m, 2H), 3.95 (s, 3H), 3.87 – 3.81 (m, 2H), 3.69 – 3.58 (m, 6H), 3.42 – 3.38 (m, 2H). ^{13}C NMR (101 MHz, DMSO-d_6): δ 157.91, 156.87, 155.40, 153.58, 152.91, 148.97, 146.89, 129.56, 129.53, 127.51, 127.47, 126.46, 126.34, 119.43, 119.20, 117.58, 117.49, 108.69, 107.76, 101.97, 69.98, 69.67, 69.26, 68.66, 68.07, 56.07, 49.99. MS (MALDI): calculated for $C_{21}H_{22}{}^{79}BrFN_6O_4$ $[M+H]^+$ m/z 521.1; found m/z 520.8.

General Procedure for CuAAC reactions (synthesis of conjugates 7, 12, 18 and chlorin 22): The corresponding alkyne **6, 11, 17 or 11** (1 eq.) together with the respective azide **3 or 21** (1-1.5 eq.) was placed in the first round-bottom flask equipped with a magnetic stirrer. Subsequently, a solvent mixture of t-BuOH/$CHCl_3$ (2:1 v/v, 6 mL) was added to the starting compounds. The mixture in the first flask was left to stir at room temperature. Meanwhile, in the second round-bottom flask equipped with a magnetic stirrer, a catalytic system consisting of $CuSO_4 \cdot 5H_2O$ (0.2 eq.), AscNa (0.4 eq.), and the ligand TBTA (0.2 eq.) was introduced. Then, water (4 mL) was

https://doi.org/10.26434/chemrxiv-2024-qsdbb **ORCID:** https://orcid.org/0000-0001-6015-099X Content not peer-reviewed by ChemRxiv. **License:** CC BY-NC-ND 4.0

added to the catalysts, and they were left to stir for 5 minutes. Afterward, the mixture in the second flask was transferred to the first and left to stir at 50 °C until a starting alkyne disappeared (~1-1.5 hours) based on TLC analysis. The flask content was then diluted with $CHCl_3$ (100 mL) and transferred to a separating funnel with further washing with H_2O (3 × 50 mL) to remove inorganic salts. The organic layer was dried with anhydrous sodium sulfate (Na_2SO_4) and concentrated under reduced pressure. The reaction product was purified using column chromatography on silica gel.

Conjugate (7): The title compound was prepared from the alkyne **6** (0.070 g, 0.09 mmol) and the azide **3** (0.061 g, 0.11 mmol) according to the General Procedure. Purification by silica gel column chromatography ($CHCl_3$/MeOH, 100:0 - 80:20) gave the product (0.092 g, 0.05 mmol 79%) as a deep green solid. ^{1}H NMR (400 MHz, DMSO-d_6): δ 9.62 – 9.44 (m, 3H), 8.72 (s, 1H), 8.63 (s, 1H), 8.31 (t, *J* = 5.7 Hz, 1H), 8.21 (dd, *J* = 17.8, 11.6 Hz, 1H), 8.03 (s, 1H), 7.82 (s, 1H), 7.75 (s, 1H), 7.64 (dd, *J* = 10.0, 2.1 Hz, 1H), 7.52 – 7.41 (m, 2H), 6.90 (s, 1H), 6.20 (dd, *J* = 17.8, 1.9 Hz, 1H), 5.98 (dd, *J* = 11.5, 1.8 Hz, 1H), 5.43 (d, *J* = 19.1 Hz, 1H), 5.07 (d, *J* = 19.0 Hz, 1H), 4.45 (t, J = 5.2 Hz, 2H), 4.38 (q, *J* = 7.0 Hz, 1H), 4.26 (d, *J* = 6.4 Hz, 2H), 4.20 (d, *J* = 9.3 Hz, 1H), 4.14 (d, *J* = 3.4 Hz, 2H), 3.88 (s, 3H), 3.84 – 3.74 (m, 4H), 3.74 – 3.68 (m, 3H), 3.65 (s, 3H), 3.61 – 3.53 (m, 1H), 3.50 (s, 3H), 3.35 (s, 3H), 2.36 (s, 6H), 2.11 – 2.01 (m, 2H), 1.66 (t, *J* = 7.6 Hz, 3H), 1.56 (d, *J* = 7.1 Hz, 3H). ^{13}C NMR (101 MHz, DMSO-d_6): δ 173.33, 171.83, 169.91, 165.03, 162.78, 157.89, 156.82, 155.39, 153.48, 152.77, 151.53, 148.87, 148.18, 146.54, 145.99, 144.71, 143.91, 143.13, 141.41, 140.63, 138.53, 137.15, 133.98, 133.01, 132.15, 130.67, 129.56, 127.50, 126.36, 123.09, 119.42, 119.19, 119.12, 117.64, 108.55, 107.42, 101.92, 101.62, 99.92, 93.11, 79.18, 69.74, 69.52, 68.75, 68.54, 68.03, 58.02, 56.03, 51.54, 49.26, 46.29, 45.24, 34.11, 32.26, 22.75, 18.86, 17.87, 12.27, 11.66, 10.91. MS (MALDI): calculated for $C_{63}H_{71}BrFN_{13}O_8Zn$ $[M]^+$ m/z 1301.4; found m/z 1301.1.

Conjugate (12): The title compound was prepared from the alkyne **11** (0.085 g, 0.12 mmol) and the azide **3** (0.073 g, 0.14 mmol) according to the General Procedure. Purification by silica gel column chromatography ($CHCl_3$/MeOH, 100:0 – 95:5) gave the product (0.115 g, 0.09 mmol,

https://doi.org/10.26434/chemrxiv-2024-qsdbb **ORCID:** https://orcid.org/0000-0001-6015-099X Content not peer-reviewed by ChemRxiv. **License:** CC BY-NC-ND 4.0

78%) as a deep green solid. ^{1}H NMR (400 MHz, DMSO-d_6): δ 9.51 (s, 1H), 9.50 (s, 1H), 9.46 (s, 1H), 9.34 (t, *J* = 5.7 Hz, 1H), 8.64 (s, 1H), 8.26 (s, 1H), 8.21 (dd, *J* = 17.9, 11.6 Hz, 1H), 7.65 – 7.58 (m, 2H), 7.45 – 7.34 (m, 2H), 7.19 (s, 1H), 6.35 – 6.14 (m, 2H), 6.00 (dd, *J* = 11.5, 1.8 Hz, 1H), 5.39 (d, *J* = 19.2 Hz, 1H), 5.10 (d, J = 19.3 Hz, 1H), 4.81 (dd, *J* = 14.8, 5.7 Hz, 1H), 4.71 (s, 1H), 4.67 (t, *J* = 5.2 Hz, 2H), 4.42 (q, *J* = 7.1 Hz, 1H), 4.29 (d, *J* = 9.4 Hz, 1H), 4.13 (s, 2H), 3.95 (t, *J* = 5.3 Hz, 2H), 3.89 – 3.84 (m, 2H), 3.82 (s, 3H), 3.81 – 3.74 (m, 2H), 3.70 (s, 3H), 3.61 (s, 3H), 3.52 (s, 3H), 3.28 (s, 3H), 2.04 (q, *J* = 10.9 Hz, 2H), 1.64 (t, *J* = 7.5 Hz, 3H), 1.56 (d, *J* = 7.0 Hz, 3H). ^{13}C NMR (101 MHz, DMSO-d_6): δ 173.28, 173.20, 170.06, 165.08, 161.98, 157.83, 156.69, 155.33, 153.41, 152.34, 151.75, 148.79, 148.04, 146.22, 145.66, 145.03, 144.08, 143.14, 141.26, 140.79, 138.92, 137.33, 133.44, 133.12, 132.34, 130.63, 129.55, 129.53, 128.74, 127.73, 127.51, 127.48, 126.11, 125.99, 123.67, 119.43, 119.27, 119.20, 117.80, 117.71, 108.19, 106.58, 102.06, 101.87, 101.77, 99.98, 93.05, 70.02, 69.88, 69.12, 68.73, 68.18, 55.98, 52.01, 51.61, 51.22, 49.57, 46.09, 37.34, 35.31, 30.70, 29.88, 29.03, 22.73, 18.83, 17.82, 12.30, 11.62, 10.91. MS (MALDI): calculated for $C_{60}H_{63}BrFN_{11}O_9Zn$ $[M]^+$ m/z 1245.3; found m/z 1245.3.

Conjugate (18): The title compound was prepared from the alkyne **17** (0.055 g, 0.08 mmol) and the azide **3** (0.047 g, 0.09 mmol) according to the General Procedure. Purification by silica gel column chromatography ($CHCl_3$/MeOH, 100:0 – 95:5) gave the product (0.074 g, 0.06 mmol, 72%) as a deep green solid. ^{1}H NMR (400 MHz, DMSO-d_6): δ 9.70 (s, 1H), 9.65 (s, 1H), 9.54 – 9.41 (m, 2H), 8.95 (s, 1H), 8.32 (s, 1H), 8.31 (s, 1H), 8.27 – 8.15 (m, 2H), 7.72 (s, 1H), 7.63 (dd, *J* = 9.9, 2.1 Hz, 1H), 7.51 – 7.38 (m, 2H), 7.18 (s, 1H), 6.24 (d, *J* = 17.8 Hz, 1H), 6.05 (d, *J* = 11.6 Hz, 1H), 5.35 (d, *J* = 19.2 Hz, 1H), 5.03 (d, *J* = 19.2 Hz, 1H), 4.87 – 4.68 (m, 2H), 4.69 – 4.55 (m, 3H), 4.41 (d, *J* = 9.6 Hz, 1H), 4.23 (br.s, 2H), 3.93 (t, *J* = 5.3 Hz, 2H), 3.85 (s, 3H), 3.84 – 3.73 (m, 3H), 3.69 (s, 3H), 3.66 (s, 3H), 3.55 (s, 3H), 2.72 – 2.59 (m, 1H), 2.36 – 2.25 (m, 1H), 2.02 – 1.89 (m, 1H), 1.62 (t, *J* = 7.6 Hz, 2H), 1.58 (d, *J* = 7.0 Hz, 3H). ^{13}C NMR (101 MHz, DMSO-d_6): δ 173.03, 172.42, 168.54, 156.77, 156.50, 155.31, 153.97, 153.50, 152.83, 148.88, 146.82, 144.63, 143.27, 140.25, 139.85, 138.80, 137.96, 137.06, 135.58, 135.42, 133.51, 132.88, 132.81, 132.21,

https://doi.org/10.26434/chemrxiv-2024-qsdbb **ORCID:** https://orcid.org/0000-0001-6015-099X Content not peer-reviewed by ChemRxiv. **License:** CC BY-NC-ND 4.0

129.68, 129.41, 127.43, 127.40, 126.41, 126.29, 123.57, 120.69, 119.37, 119.14, 117.48, 117.39, 108.63, 107.70, 103.86, 103.35, 101.89, 95.37, 79.17, 69.87, 69.68, 69.00, 68.66, 68.04, 55.99, 51.84, 51.68, 51.33, 49.47, 45.95, 36.96, 35.26, 30.02, 28.27, 22.18, 18.72, 17.50, 12.23, 11.61, 10.86. MS (MALDI): calculated for $C_{60}H_{63}BrFN_{11}O_9Pd$ $[M]^+$ m/z 1286.3; found m/z 1286.1.

Chlorin (22): The title compound was prepared from the alkyne **11** (0.233 g, 0.32 mmol) and the azide **21** (0.073 g, 0.38 mmol) according to the General Procedure. Purification by silica gel column chromatography ($CHCl_3$/MeOH, 91:1 – 95:5) gave the product (0.223 g, 0.24 mmol, 76%) as a deep green solid. ^{1}H NMR: (400 MHz, DMSO-d_6) δ 9.51 (s, 1H), 9.50 (s, 1H), 9.30 (t, *J* = 5.6 Hz, 1H), 8.65 (s, 1H), 8.22 (q, *J* = 11.8 Hz, 1H), 8.08 (s, 1H), 6.22 (dd, *J* = 17.8, 1.9 Hz, 1H), 6.00 (dd, *J* = 11.5, 1.8 Hz, 1H), 5.59 (s, 2H), 5.26 (m, 2H), 4.64 (t, *J* = 5.2 Hz, 2H), 4.43 (q, *J* = 7.2 Hz, 1H), 4.30 (d, J = 9.1 Hz, 1H), 3.91 (t, *J* = 5.3 Hz, 2H), 3.81 (q, *J* = 7.5 Hz, 2H), 3.65 (s, 3H), 3.62 (s, 3H), 3.62 – 3.59 (m, 2H), 3.57 – 3.55 (m, 2H), 3.54 (s, 3H), 3.53 – 3.50 (m, 2H), 3.44 – 3.41 (m, 2H), 3.37 (s, 3H), 3.29 (s, 3H), 3.21 (s, 3H), 2.63 – 2.52 (m, 2H), 2.15 – 2.05 (m, 2H), 1.67 (t, *J* = 7.6 Hz, 3H), 1.60 (d, *J* = 7.1 Hz, 3H). ^{13}C NMR: (101 MHz, DMSO-d_6) δ 173.28, 173.25, 170.02, 165.02, 162.05, 151.66, 148.05, 146.10, 144.88, 144.03, 143.68, 143.09, 141.29, 140.72, 138.78, 137.24, 136.21, 133.43, 133.03, 132.26, 130.65, 128.73, 128.02, 127.71, 124.17, 123.56, 119.20, 101.96, 101.74, 99.92, 93.01, 71.27, 69.70, 69.68, 69.61, 68.97, 58.03, 52.70, 51.95, 51.61, 51.23, 49.45, 46.93, 46.09, 37.36, 35.28, 29.94, 29.16, 22.80, 18.87, 17.87, 12.28, 11.66, 10.92. MS (MALDI-TOF): calculated for $C_{46}H_{56}N_8O_8Zn$ $[M]^+$ m/z 912.4; found m/z 912.2

General Procedure for aminomethylation reactions (synthesis of conjugates 8, 13, 19 and chlorin 23): Into a round-bottom flask equipped with a magnetic stirrer, containing a solution of the compound **7, 12, 18 or 22** (1 eq.) dissolved in AcOH/THF (8-10 mL), an excess of bis(dimethylamino)methane (~80-100 eq.) was added. The mixture was left stirring for 1 hour. Subsequently, the mixture was diluted with $CHCl_3$ (100 mL) and transferred to a separating funnel with further washing using 2% NaOH (3 × 100 mL) and H_2O (1 × 100 mL). The organic layer was

https://doi.org/10.26434/chemrxiv-2024-qsdbb **ORCID:** https://orcid.org/0000-0001-6015-099X Content not peer-reviewed by ChemRxiv. **License:** CC BY-NC-ND 4.0

dried with a drying agent (Na_2SO_4) and concentrated under reduced pressure. The reaction product was isolated using column chromatography on silica gel.

Conjugate (8): The title compound was prepared from the conjugate **7** (0.040 g, 0.03 mmol) and bis(dimethylamino)methane (0.251 g, 2.45 mmol) according to the General Procedure. Purification by silica gel column chromatography ($CHCl_3$/MeOH-Et_3N, 98:1:1 – 94:5:1) gave the product (0.028 g, 0.03 mmol, 65%) as a deep green solid. ^{1}H NMR (400 MHz, DMSO-d_6): δ 9.61 (s, 1H), 9.57 – 9.45 (m, 2H), 8.70 (t, *J* = 6.2 Hz, 1H), 8.59 (s, 1H), 8.32 (s, 1H), 8.02 (d, *J* = 27.4 Hz, 1H), 7.83 (s, 1H), 7.74 (d, *J* = 4.1 Hz, 1H), 7.64 (d, *J* = 9.9 Hz, 1H), 7.52 – 7.40 (m, 2H), 7.22 – 7.12 (m, 1H), 6.90 (d, *J* = 23.9 Hz, 1H), 5.44 (d, *J* = 19.0 Hz, 1H), 5.06 (d, *J* = 19.0 Hz, 1H), 4.45 (t, *J* = 5.2 Hz, 2H), 4.43 – 4.33 (m, 1H), 4.26 (d, *J* = 5.6 Hz, 2H), 4.20 (d, *J* = 10.1 Hz, 1H), 4.15 (s, 2H), 3.88 (s, 3H), 3.85 – 3.74 (m, 5H), 3.74 – 3.68 (m, 3H), 3.65 (s, 3H), 3.60 – 3.46 (m, 6H), 2.79 – 2.70 (m, 1H), 2.66 (t, *J* = 7.0 Hz, 2H), 2.47 – 2.36 (m, 3H), 2.32 (s, 6H), 2.19 (s, 6H), 2.16 (d, *J* = 11.7 Hz, 3H), 2.11 – 1.99 (m, 1H), 1.67 (t, *J* = 7.6 Hz, 3H), 1.58 – 1.52 (m, 3H). ^{13}C NMR (101 MHz, DMSO-d_6): δ 173.31, 171.81, 170.00, 169.88, 165.04, 162.73, 157.89, 156.82, 155.38, 153.49, 152.77, 151.04, 148.88, 148.14, 145.62, 144.73, 144.70, 143.14, 142.79, 142.72, 141.39, 140.61, 138.56, 138.43, 134.07, 133.46, 133.28, 132.76, 129.54, 127.50, 127.46, 126.36, 123.10, 119.42, 119.19, 117.63, 117.55, 107.45, 101.90, 79.17, 69.74, 69.53, 68.76, 68.54, 68.03, 58.13, 56.02, 55.49, 51.53, 49.26, 45.37, 45.18, 37.71, 34.10, 22.74, 22.68, 21.10, 21.07, 18.86, 17.86, 11.64, 11.25, 11.22, 10.86. MS (MALDI): calculated for $C_{69}H_{85}BrFN_{15}O_8Zn$ $[M+H]^+$ m/z 1417.5; found m/z 1417.3.

Conjugate (13): The title compound was prepared from the conjugate **12** (0.050 g, 0.04 mmol) and bis(dimethylamino)methane (0.327 g, 3.21 mmol) according to the General Procedure. Purification by silica gel column chromatography ($CHCl_3$/MeOH-Et_3N, 98:1:1 – 94:5:1) gave the product (0.032 g, 0.02 mmol, 59%) as a deep green solid. ^{1}H NMR (400 MHz, DMSO-d_6): δ 9.71 – 9.57 (m, 1H), 9.56 – 9.42 (m, 2H), 9.34 (s, 1H), 8.60 (s, 1H), 8.25 (s, 1H), 7.67 – 7.57 (m, 2H), 7.44 – 7.32 (m, 2H), 7.23 – 7.11 (m, 1H), 5.39 (d, *J* = 19.7 Hz, 1H), 5.09 (d, *J* = 18.6 Hz, 1H),

https://doi.org/10.26434/chemrxiv-2024-qsdbb **ORCID:** https://orcid.org/0000-0001-6015-099X Content not peer-reviewed by ChemRxiv. **License:** CC BY-NC-ND 4.0

4.86 – 4.76 (m, 1H), 4.68 (q, *J* = 8.1, 5.2 Hz, 3H), 4.40 (d, *J* = 7.2 Hz, 1H), 4.28 (d, *J* = 9.5 Hz, 1H), 4.13 (s, 2H), 3.95 (t, *J* = 5.2 Hz, 2H), 3.89 – 3.75 (m, 8H), 3.70 (br.s, 4H), 3.61 (br.s, 4H), 3.51 (br.s, 4H), 2.83 – 2.70 (m, 1H), 2.25 (br.s, 7H), 2.16 (d, *J* = 10.6 Hz, 3H), 2.10 – 1.98 (m, 2H), 1.68 – 1.61 (m, 4H), 1.57 – 1.50 (m, 4H). ^{13}C NMR (101 MHz, DMSO-d_6): δ 173.27, 173.20, 170.08, 170.01, 165.09, 161.97, 157.84, 156.68, 155.34, 153.39, 152.35, 151.25, 148.80, 148.77, 148.01, 145.87, 145.65, 145.02, 143.16, 143.00, 142.91, 141.26, 141.23, 140.78, 138.95, 138.57, 133.74, 133.50, 133.45, 132.87, 129.53, 127.48, 126.04, 123.73, 123.59, 119.48, 119.37, 119.13, 117.77, 108.25, 108.17, 106.71, 106.55, 102.10, 102.06, 101.82, 100.49, 100.39, 70.06, 70.02, 69.87, 69.12, 68.74, 68.16, 56.00, 55.41, 52.01, 51.61, 51.22, 49.57, 46.10, 45.06, 43.34, 42.40, 42.22, 40.15, 39.94, 39.73, 39.52, 39.31, 39.10, 38.89, 35.31, 29.90, 22.72, 22.67, 21.12, 21.09, 18.83, 17.82, 11.62, 11.29, 11.27, 10.87. MS (MALDI): calculated for $C_{66}H_{77}BrFN_{13}O_9Zn$ $[M+H]^+$ m/z 1363.4; found m/z 1363.0.

Conjugate (19): The title compound was prepared from the conjugate **18** (0.065 g, 0.05 mmol) and bis(dimethylamino)methane (0.443 g, 4.34 mmol) according to the General Procedure. Purification by silica gel column chromatography ($CHCl_3$/MeOH, 100:0 – 90:10) gave the product (0.045 g, 0.03 mmol, 63%) as a deep green solid. ^{1}H NMR (400 MHz, DMSO-d_6): δ 9.84 (br.s, 1H), 9.68 (s, 1H), 9.58 – 9.46 (m, 2H), 8.93 (s, 1H), 8.23 (s, 1H), 7.77 (s, 1H), 7.63 (d, *J* = 9.8 Hz, 1H), 7.52 – 7.38 (m, 2H), 7.20 (s, 1H), 7.19 – 7.13 (m, 1H), 5.36 (d, *J* = 19.1 Hz, 1H), 5.02 (d, *J* = 18.8 Hz, 1H), 4.91 – 4.69 (m, 2H), 4.68 – 4.57 (m, 4H), 4.28 – 4.19 (m, 2H), 3.93 (t, *J* = 5.2 Hz, 2H), 3.88 (s, 3H), 3.85 – 3.76 (m, 4H), 3.69 (s, 3H), 3.66 (s, 5H), 3.56 – 3.52 (m, 4H), 2.96 – 2.79 (m, 2H), 2.73 – 2.59 (m, 3H), 2.45 (s, 4H), 2.19 (d, *J* = 15.8 Hz, 3H), 2.01 – 1.88 (m, 1H), 1.63 (t, *J* = 7.5 Hz, 3H), 1.59 – 1.54 (m, 3H). ^{13}C NMR (101 MHz, DMSO-d_6): δ 173.05, 172.42, 170.01, 169.89, 168.54, 157.86, 156.84, 156.47, 155.38, 154.08, 153.55, 152.88, 148.92, 146.86, 144.62, 144.58, 142.71, 140.33, 138.95, 137.55, 133.85, 133.67, 133.58, 133.09, 132.99, 132.71, 129.48, 127.45, 126.44, 126.32, 125.95, 123.58, 119.40, 119.16, 117.53, 108.68, 107.74, 103.89, 103.47, 101.98, 95.39, 69.88, 69.68, 69.01, 68.67, 68.07, 56.06, 56.04, 51.87, 51.69, 51.35, 49.47, 48.60,

https://doi.org/10.26434/chemrxiv-2024-qsdbb **ORCID:** https://orcid.org/0000-0001-6015-099X Content not peer-reviewed by ChemRxiv. **License:** CC BY-NC-ND 4.0

45.94, 44.31, 36.97, 35.25, 30.02, 28.25, 22.18, 20.98, 18.74, 17.53, 11.61, 11.32, 10.90. MS (MALDI): calculated for $C_{66}H_{77}BrFN_{13}O_9Pd$ $[M+H]^+$ m/z 1404.4; found m/z 1404.1.

Chlorin (23): The title compound was prepared from the chlorin **22** (0.113 g, 0.12 mmol) and bis(dimethylamino)methane (1.268 g, 12.4 mmol) according to the General Procedure. Purification by silica gel column chromatography ($CHCl_3$/MeOH, 98:2 – 90:10) gave the product (0.108 g, 0.10 mmol, 85%) as a deep green solid. ^{1}H NMR (400 MHz, DMSO-d_6): δ 9.65 (s, 1H), 9.50 (s, 1H), 9.30 (t, *J* = 5.4 Hz, 1H), 8.61 (s, 1H), 8.21 (s, 1H), 7.25 – 7.08 (m, 1H), 5.47 – 5.04 (m, 2H), 4.88 – 4.67 (m, 2H), 4.64 (t, *J* = 5.2 Hz, 2H), 4.42 (d, *J* = 7.1 Hz, 1H), 4.29 (d, *J* = 9.4 Hz, 1H), 3.91 (t, *J* = 5.2 Hz, 2H), 3.85 – 3.76 (m, 2H), 3.66 (s, 3H), 3.61 (dd, *J* = 5.9, 3.3 Hz, 2H), 3.58 – 3.49 (m, 9H), 3.45 – 3.39 (m, 5H), 3.29 (s, 6H), 3.22 (s, 3H), 2.23 (s, 6H), 1.66 (dt, *J* = 6.8, 3.3 Hz, 3H), 1.59 (dd, *J* = 6.8, 3.1 Hz, 3H). ^{13}C NMR: (101 MHz, DMSO-d_6) δ 173.25, 169.99, 165.04, 162.05, 145.74, 144.87, 143.11, 142.91, 140.71, 138.82, 133.44, 132.79, 123.55, 101.76, 79.17, 71.27, 69.70, 69.68, 69.61, 68.97, 58.03, 55.45, 51.96, 51.61, 51.23, 49.45, 46.11, 45.08, 35.28, 30.69, 29.97, 29.14, 22.77, 21.08, 18.87, 17.86, 11.66, 11.25, 10.87. MS (MALDI-TOF): calculated for $C_{52}H_{71}N_{10}O_8Zn$ $[M+H]^+$ m/z 1029.6; found m/z 1029.0

General Procedure for quaternization reactions (synthesis of conjugates 9, 14, 16, 20 and chlorins 24, 26): Into a round-bottom flask equipped with a magnetic stirrer and containing the conjugate **9, 14, 16, 20** or chlorins **24, 26** (1 eq.) dissolved in THF (~5 mL) an excess of CH_3I (~60-100 eq.) was added. The mixtures were left stirring for 15 minutes. The resulting reaction precipitate was collected and washed with a small amount of THF. The obtained product was dried under reduced pressure.

Conjugate (9): The title compound was prepared from the conjugate **8** (0.040 g, 0.03 mmol) and CH_3I (0.400 g, 2.82 mmol) according to the General Procedure. The product was obtained as a deep green solid (0.053 g, quantitative). ^{1}H NMR (400 MHz, DMSO-d_6): δ 9.70 – 9.46 (m, 3H), 9.18 (s, 1H), 8.63 (s, 1H), 8.35 (s, 1H), 8.20 – 7.97 (m, 1H), 7.86 (s, 1H), 7.74 (s, 1H), 7.64 (d, *J* = 9.7 Hz, 1H), 7.46 (s, 2H), 7.24 – 7.07 (m, 1H), 6.94 (d, *J* = 19.6 Hz, 1H), 5.37 (d, *J* = 18.7 Hz,

https://doi.org/10.26434/chemrxiv-2024-qsdbb **ORCID:** https://orcid.org/0000-0001-6015-099X Content not peer-reviewed by ChemRxiv. **License:** CC BY-NC-ND 4.0

1H), 5.08 (d, J = 18.5 Hz, 1H), 4.52 – 4.36 (m, 3H), 4.32 – 4.09 (m, 5H), 4.08 – 3.96 (m, 1H), 3.95 – 3.47 (m, 25H), 3.13 (s, 12H), 2.92 – 2.77 (m, 1H), 2.29 – 2.12 (m, 4H), 2.12 – 1.97 (m, 3H), 1.66 (t, J = 7.5 Hz, 3H), 1.60 – 1.52 (m, 3H). ^{13}C NMR (101 MHz, DMSO-d_6): δ 173.23, 171.84, 169.89, 162.94, 157.91, 156.84, 155.41, 153.48, 152.82, 152.22, 150.98, 148.89, 144.67, 143.34, 140.93, 133.95, 132.82, 129.55, 127.53, 127.50, 123.12, 119.44, 119.20, 101.94, 101.82, 69.75, 69.54, 68.77, 68.56, 68.06, 63.63, 62.73, 56.06, 52.78, 52.39, 51.77, 49.29, 34.11, 22.70, 21.06, 17.88, 11.84, 11.39, 11.02.

Conjugate (14): The title compound was prepared from the conjugate **13** (0.030 g, 0.02 mmol) and CH_3I (0.282 g, 1.98 mmol) according to the General Procedure. The product was obtained as a deep green solid (0.036 g, quantitative). ^{1}H NMR (400 MHz, DMSO-d_6): δ 9.66 – 9.56 (m, 1H), 9.57 – 9.44 (m, 2H), 9.34 (t, J = 5.9 Hz, 1H), 8.68 – 8.60 (m, 1H), 8.25 (s, 1H), 7.69 – 7.57 (m, 2H), 7.45 – 7.31 (m, 2H), 7.22 – 7.09 (m, 1H), 5.39 (d, J = 19.3 Hz, 1H), 5.09 (d, J = 19.0 Hz, 1H), 4.88 – 4.71 (m, 1H), 4.67 (t, J = 5.2 Hz, 2H), 4.41 (d, J = 7.3 Hz, 1H), 4.29 (d, J = 9.3 Hz, 1H), 4.16 (br.s, 2H), 3.95 (t, J = 5.1 Hz, 2H), 3.90 – 3.75 (m, 8H), 3.70 (br.s, 4H), 3.61 (s, 3H), 3.45 (d, J = 2.9 Hz, 1H), 3.38 (d, J = 2.6 Hz, 2H), 3.12 (br.s, 12H), 2.92 – 2.81 (m, 1H), 2.21 (d, J = 12.7 Hz, 3H), 2.12 – 1.96 (m, 3H), 1.74 – 1.61 (m, 4H), 1.60 – 1.50 (m, 4H). ^{13}C NMR (101 MHz, DMSO-d_6): δ 173.27, 173.19, 169.96, 169.89, 165.02, 162.16, 157.85, 156.73, 155.35, 153.44, 151.42, 150.90, 148.83, 148.17, 145.89, 144.97, 143.36, 142.37, 142.23, 141.45, 140.81, 139.10, 136.97, 133.91, 133.83, 133.63, 133.61, 133.20, 133.17, 129.54, 127.52, 127.49, 126.02, 123.66, 119.43, 119.20, 117.79, 117.70, 108.25, 106.72, 101.82, 93.13, 69.97, 69.88, 69.10, 68.72, 68.18, 56.02, 56.02, 52.38, 52.00, 51.63, 51.25, 49.57, 48.60, 46.14, 35.28, 34.20, 30.38, 29.91, 29.05, 22.71, 21.06, 18.82, 17.84, 11.62, 11.50, 11.42, 11.03.

Conjugate (16): The title compound was prepared from the conjugate **15** (0.035 g, 0.02 mmol) and CH_3I (0.343 g, 2.42 mmol) according to the General Procedure. The product was obtained as a deep green solid (0.041 g, quantitative). ^{1}H NMR (400 MHz, DMSO-d_6): δ 10.02 – 9.38 (m, 4H), 9.23 – 8.95 (m, 1H), 8.65 – 8.43 (m, 1H), 8.38 – 8.18 (m, 2H), 7.80 (s, 1H), 7.72 – 7.59 (m, 1H),

https://doi.org/10.26434/chemrxiv-2024-qsdbb **ORCID:** https://orcid.org/0000-0001-6015-099X Content not peer-reviewed by ChemRxiv. **License:** CC BY-NC-ND 4.0

7.22 (s, 1H), 7.09 – 6.87 (m, 1H), 5.63 – 5.17 (m, 2H), 4.82 (br.s, 2H), 4.76 – 4.48 (m, 6H), 4.40 – 4.21 (m, 3H), 4.03 – 3.78 (m, 11H), 3.74 – 3.61 (m, 9H), 3.60 – 3.41 (m, 13H), 2.37 – 2.15 (m, 2H), 2.06 – 1.80 (m, 3H), 1.80 – 1.54 (m, 8H). ^{13}C NMR (101 MHz, DMSO-d_6): δ 154.02, 153.36, 149.40, 147.31, 129.98, 127.93, 126.87, 126.75, 119.88, 119.65, 110.83, 109.14, 108.20, 103.09, 102.42, 70.34, 70.24, 70.14, 69.46, 69.14, 68.55, 58.41, 56.53, 52.75, 51.79, 49.95, 37.99, 37.07, 36.25, 35.76, 33.19, 29.83, 23.64, 19.19, 18.06, 13.15, 12.15, 11.48.

Conjugate (20): The title compound was prepared from the conjugate **19** (0.030 g, 0.02 mmol) and CH_3I (0.273 g, 1.92 mmol) according to the General Procedure. The product was obtained as a deep green solid (0.035 g, quantitative). ^{1}H NMR (400 MHz, DMSO-d_6): δ 9.83 (s, 1H), 9.74 – 9.61 (m, 1H), 9.56 – 9.44 (m, 2H), 8.97 (s, 1H), 8.32 (s, 1H), 8.23 (s, 1H), 7.95 – 7.61 (m, 2H), 7.56 – 7.40 (m, 2H), 7.33 – 7.08 (m, 2H), 5.34 (d, *J* = 19.3 Hz, 1H), 5.02 (d, *J* = 18.6 Hz, 1H), 4.89 – 4.70 (m, 2H), 4.71 – 4.55 (m, 4H), 4.50 – 4.19 (m, 4H), 4.00 – 3.76 (m, 10H), 3.77 – 3.63 (m, 10H), 3.57 – 3.53 (m, 4H), 3.22 – 3.04 (m, 9H), 2.96 – 2.80 (m, 1H), 2.71 – 2.59 (m, 1H), 2.23 (d, *J* = 16.6 Hz, 3H), 2.07 – 1.89 (m, 1H), 1.69 – 1.61 (m, 3H), 1.60 – 1.54 (m, 3H). ^{13}C NMR (101 MHz, DMSO-d_6): δ 174.22, 173.07, 172.43, 170.97, 169.91, 168.48, 156.87, 156.51, 155.38, 154.19, 153.58, 152.84, 148.96, 144.63, 144.59, 142.57, 140.37, 139.00, 137.56, 136.78, 133.91, 133.09, 132.96, 129.50, 127.48, 123.59, 119.42, 119.19, 108.67, 103.89, 101.98, 95.51, 79.19, 69.93, 69.89, 69.78, 69.69, 69.01, 68.67, 68.48, 68.10, 67.03, 62.49, 56.50, 56.07, 52.42, 51.90, 51.70, 51.38, 49.50, 45.95, 36.97, 35.24, 30.02, 28.28, 25.13, 22.19, 21.00, 18.74, 17.55, 11.62, 11.47, 11.04.

Chlorin (24): The title compound was prepared from the conjugate **23** (0.030 g, 0.03 mmol) and CH_3I (0.414 g, 2.92 mmol) according to the General Procedure. The product was obtained as a deep green solid (0.038 g, quantitative). ^{1}H NMR (400 MHz, DMSO-d_6): δ 9.70 (s, 1H), 9.52 (s, 1H), 9.31 (t, *J* = 5.3 Hz, 1H), 8.65 (s, 1H), 8.22 (s, 1H), 7.24 – 7.06 (m, 1H), 5.51 – 5.03 (m, 2H), 4.77 (d, *J* = 16.0 Hz, 2H), 4.64 (t, *J* = 5.2 Hz, 2H), 4.43 (d, *J* = 6.9 Hz, 1H), 4.30 (d, *J* = 8.7 Hz, 1H), 3.91 (t, *J* = 5.2 Hz, 2H), 3.86 – 3.75 (m, 2H), 3.65 (s, 3H), 3.63 – 3.59 (m, 3H), 3.58 – 3.48

https://doi.org/10.26434/chemrxiv-2024-qsdbb **ORCID:** https://orcid.org/0000-0001-6015-099X Content not peer-reviewed by ChemRxiv. **License:** CC BY-NC-ND 4.0

(m, 10H), 3.45 – 3.41 (m, 3H), 3.41 – 3.38 (m, 3H), 3.30 (s, 3H), 3.22 (s, 3H), 3.14 (s, 9H), 2.56 (t, *J* = 5.4 Hz, 2H), 2.17 – 2.06 (m, 2H), 1.67 (td, *J* = 7.4, 3.3 Hz, 3H), 1.59 (t, *J* = 6.1 Hz, 3H). 13C NMR (101 MHz, DMSO-d6): δ 173.26, 169.90, 165.03, 162.23, 148.18, 145.82, 144.85, 143.33, 142.35, 142.21, 141.46, 140.78, 136.94, 133.83, 133.60, 133.15, 123.58, 102.12, 97.18, 79.20, 71.29, 69.71, 69.63, 68.98, 68.28, 65.71, 58.06, 52.42, 51.96, 51.65, 51.28, 49.48, 48.61, 46.16, 40.15, 39.94, 39.73, 39.52, 39.31, 39.10, 38.89, 37.39, 35.27, 34.43, 33.17, 29.96, 27.43, 23.31, 22.80, 21.75, 21.10, 18.87, 17.90, 11.69, 11.07.

Conjugate (26): The title compound was prepared from the conjugate **23** (0.012 g, 0.01 mmol) and CH_3I (0.153 g, 1.08 mmol) according to the General Procedure. The product was obtained as a deep green solid (0.015 g, quantitative). ^{1}H NMR: (400 MHz, DMSO-d_6): δ 9.94 (s, 1H), 9.79 (s, 1H), 9.65 (s, 1H), 9.17 (s, 1H), 8.56 (dd, *J* = 27.9, 15.7 Hz, 1H), 8.26 (s, 1H), 6.99 (qd, *J* = 15.5, 7.5 Hz, 1H), 5.59 – 5.30 (m, 2H), 4.88 – 4.72 (m, 2H), 4.69 – 4.57 (m, 5H), 4.00 – 3.87 (m, 2H), 3.68 – 3.50 (m, 12H), 3.47 – 3.41 (m, 5H), 3.38 (s, 3H), 3.35 (s, 3H), 3.25 – 3.16 (m, 9H), 1.77 – 1.67 (m, 6H). ^{13}C NMR (101 MHz, DMSO-d_6): δ 173.05, 150.16, 144.36, 142.02, 140.25, 134.56, 123.73, 97.16, 71.30, 69.71, 69.68, 69.63, 68.96, 65.70, 58.07, 52.28, 49.48, 48.60, 38.07, 37.50, 35.27, 33.16, 29.64, 28.98, 28.26, 26.35, 23.29, 22.35, 18.76, 17.63, 13.87, 12.74, 11.74, 11.10, 10.67.

General Procedure for insertion of In into photosensitizers (synthesis of conjugates 9, 14, 16, 20 and chlorins 24, 26): In a round-bottom flask equipped with a magnetic stirrer, the zinc-complex **13, 23** (1 eq.) was added with TFA (5 mL). The reaction mixture was then stirred for 15 minutes at room temperature. Removal of zinc from the chlorin core was monitored by TLC. Then, the contents of the flask were diluted with $CHCl_3$ (100 mL) and transferred to a separating funnel with subsequent washing with 2% NaOH (3 × 100 mL) and H_2O (1 × 100 mL). The organic layer was dried with a drying agent (Na_2SO_4) and concentrated under reduced pressure. The resulting product was then dissolved in CH_3COOH (16 mL) and CH_3COONa (16 eq.) was added. Subsequently, $InCl_3$ (6 eq.) was introduced into the flask, and the mixture was stirred at 118°C for

https://doi.org/10.26434/chemrxiv-2024-qsdbb **ORCID:** https://orcid.org/0000-0001-6015-099X Content not peer-reviewed by ChemRxiv. **License:** CC BY-NC-ND 4.0

3 hours. The insertion of indium into the chlorin core was monitored by TLC. Then, the reaction mixture was diluted with $CHCl_3$ (100 mL) and transferred to a separating funnel with subsequent washing with 2% NaOH (3 × 100 mL) and H_2O (1 × 100 mL). The organic layer was dried with a drying agent (Na_2SO_4) and concentrated under reduced pressure. The product was isolated using column chromatography on silica gel.

Conjugate (15): The title compound was prepared from the conjugate **13** (0.140 g, 0.10 mmol) according to the General Procedure. Purification by silica gel column chromatography ($CHCl_3$/MeOH-Et_3N 99:0:1-57:40:3) gave the product (0.040 g, 0.05 mmol, 48%) as a deep green solid. ^{1}H NMR (400 MHz, DMSO-d_6): δ 9.97 – 9.39 (m, 4H), 9.04 – 8.83 (m, 1H), 8.60 – 8.22 (m, 2H), 7.85 – 7.58 (m, 2H), 7.43 (s, 2H), 7.21 (s, 1H), 7.08 – 6.74 (m, 1H), 5.89 – 5.74 (m, 1H), 5.70 – 4.99 (m, 2H), 4.97 – 4.39 (m, 8H), 4.25 (s, 3H), 4.07 – 3.77 (m, 10H), 3.68 (br.s, 4H), 3.60 – 3.47 (m, 5H), 3.04 (br.s, 1H), 2.30 – 2.14 (m, 2H), 1.76 – 1.48 (m, 6H). ^{13}C NMR (101 MHz, DMSO-d_6): δ 156.83, 153.55, 152.90, 148.92, 146.87, 144.63, 142.19, 134.51, 129.45, 127.86, 127.46, 126.44, 126.25, 123.65, 119.41, 119.17, 117.45, 108.69, 107.74, 101.96, 69.90, 69.70, 69.02, 68.69, 68.10, 66.28, 65.65, 56.01, 51.80, 51.27, 49.66, 49.49, 45.14, 35.29, 29.42, 18.73, 17.56, 12.62, 11.66, 10.98. MS (MALDI): calculated for $C_{66}H_{77}BrClFInN_{13}O_9$ $[M\text{-}Cl]^+$ m/z 1412.4; found m/z 1412.9.

Chlorin (25): The title compound was prepared from the conjugate **23** (0.113 g, 0.12 mmol) according to the General Procedure. Purification by silica gel column chromatography ($CHCl_3$/MeOH-Et_3N 95:5:0-58:40:2) gave the product (0.021 g, 0.05 mmol, 53%) as a deep green solid. ^{1}H NMR (400 MHz, DMSO-d_6): δ 9.87 (s, 1H), 9.76 (s, 1H), 9.61 (s, 1H), 9.06 (s, 1H), 8.25 (s, 1H), 6.87 – 6.73 (m, 1H), 5.45 (s, 1H), 5.30 (s, 1H), 4.92 – 4.76 (m, 2H), 4.65 (t, J = 5.1 Hz, 2H), 4.01 – 3.85 (m, 2H), 3.92 (t, J = 5.1 Hz, 2H), 3.67 – 3.60 (m, 5H), 3.59 – 3.50 (m, 8H), 3.47 – 3.43 (m, 6H), 3.41 (s, 3H), 3.23 (s, 3H), 2.47 (s, 6H), 1.71 (t, J = 7.1 Hz, 3H). ^{13}C NMR (101 MHz, DMSO-d_6): δ 172.95, 169.03, 144.66, 141.95, 141.35, 134.90, 134.26, 132.90, 124.84, 123.67, 102.81, 79.20, 71.32, 69.74, 69.72, 69.66, 68.99, 62.40, 58.09, 51.82, 51.28, 49.51, 45.28,

https://doi.org/10.26434/chemrxiv-2024-qsdbb **ORCID:** https://orcid.org/0000-0001-6015-099X Content not peer-reviewed by ChemRxiv. **License:** CC BY-NC-ND 4.0

45.16, 38.10, 37.51, 36.24, 35.35, 31.57, 31.32, 29.65, 29.02, 28.72, 28.28, 23.06, 22.37, 22.12, 18.80, 17.88, 17.69, 13.90, 12.32, 11.69, 10.94, 10.69.

Chlorin (11): In a round-bottom flask equipped with a stirrer, MePheid-*a* **10** (0.150 g, 0.25 mmol) was placed and dissolved in $CHCl_3$ (5 mL). An excess of propargyl amine (0.550 g, 10 mmol) was then added, and the mixture was stirred for approximately 24 hours at room temperature until MePheid-*a* disappeared on the TLC plate. Subsequently, the flask's content was diluted with $CHCl_3$ (100 mL) and transferred to a separating funnel, followed by washing with H_2O (3 × 50 mL) to remove the unreacted propargyl amine. The organic layer was dried with Na_2SO_4, concentrated under reduced pressure, and then dissolved in $CHCl_3$/MeOH 3:1 (5 mL). Zinc acetate dihydrate (0.275 g, 1.25 mmol) was added to the solution, and the mixture was stirred until the dark spot of pheophorbide disappeared on the TLC plate, forming a dark green spot corresponding to the zinc complex. The solvent was then removed under reduced pressure. The residue was dissolved in $CHCl_3$ (100 mL), washed with H_2O (3 × 50 mL), dried (Na_2SO_4), and concentrated again under reduced pressure. Purification by silica gel column chromatography ($CHCl_3$/MeOH 100:0 – 98:2) gave the product (0.160 g, 0.22 mmol, 89%) as a deep green solid. ^{1}H NMR (400 MHz, DMSO-d_6): δ 9.52 (s, 1H), 9.51 (s, 1H), 9.26 (t, J = 5.6 Hz, 1H), 8.65 (s, 1H), 8.22 (dd, J = 17.8, 11.5 Hz, 1H), 6.22 (dd, J = 17.8, 1.8 Hz, 1H), 6.00 (dd, J = 11.5, 1.8 Hz, 1H), 5.38 (d, J = 19.1 Hz, 1H), 5.12 (d, J = 19.2 Hz, 1H), 4.43 (q, J = 7.1 Hz, 1H), 4.30 (d, J = 8.3 Hz, 3H), 3.82 (q, J = 7.6 Hz, 2H), 3.67 (s, 3H), 3.54 (s, 3H), 2.64 – 2.54 (m, 1H), 2.11 (d, J = 10.5 Hz, 2H), 1.81 – 1.72 (m, 1H), 1.67 (t, J = 7.5 Hz, 3H), 1.59 (d, J = 7.1 Hz, 3H). ^{13}C NMR (101 MHz, DMSO-d_6): δ 173.33, 173.30, 169.94, 165.15, 162.08, 151.74, 147.88, 146.22, 144.13, 143.11, 141.22, 140.83, 138.93, 137.30, 133.08, 133.02, 132.35, 130.66, 119.26, 101.99, 101.87, 99.92, 93.05, 81.24, 73.00, 51.96, 51.67, 51.26, 29.96, 29.19, 28.84, 22.81, 18.88, 17.91, 12.30, 11.59, 10.93. MS (MALDI): calculated for $C_{39}H_{41}N_5O_5Zn$ $[M]^+$ m/z 723.2; found m/z 723.1.

Chlorin (17): In a round-bottom flask equipped with a magnetic stirrer, a reflux condenser, and containing a solution of 0.1 g of MePheid-*a* **10** (0.100 g, 0.16 mmol) in MeCN (60 mL), $Pd(OAc)_2$

https://doi.org/10.26434/chemrxiv-2024-qsdbb **ORCID:** https://orcid.org/0000-0001-6015-099X Content not peer-reviewed by ChemRxiv. **License:** CC BY-NC-ND 4.0

(0.059 g, 0.26 mmol) was added. The reaction mixture was stirred at 85°C for 3 hours. The formation of the palladium complex of MePheid-*a* was monitored using TLC. After concentration under reduced pressure, the mixture was diluted with $CHCl_3$ (100 mL) and transferred to a separating funnel, followed by washing with H_2O (3 × 100 mL). The organic layer was dried with Na_2SO_4 and concentrated under reduced pressure. The resulting residue was dissolved in $CHCl_3$ (5 mL), and propargyl amine (0.354 g, 6.43 mmol) was added, followed by stirring for 48 hours. Subsequently, the reaction mixture was diluted with $CHCl_3$ (100 mL) and transferred to a separating funnel, followed by washing with H_2O (3 × 100 mL). The organic layer was dried with Na_2SO_4 and concentrated under reduced pressure. The reaction product was purified using column chromatography on silica gel with $CHCl_3$ as the eluent. Purification by silica gel column chromatography ($CHCl_3$) gave the product (0.063 g, 0.08 mmol, 52%) as a deep green solid. ^{1}H NMR (400 MHz, $CDCl_3$): δ 9.57 (s, 1H), 9.48 (s, 1H), 8.65 (s, 1H), 7.98 (dd, *J* = 17.8, 11.5 Hz, 1H), 6.59 (t, *J* = 5.1 Hz, 1H), 6.16 (dd, *J* = 17.8, 1.7 Hz, 1H), 6.03 (dd, *J* = 11.5, 1.6 Hz, 1H), 5.36 (d, *J* = 19.2 Hz, 1H), 5.00 (d, *J* = 19.1 Hz, 1H), 4.63 – 4.53 (m, 1H), 4.51 – 4.40 (m, 2H), 4.39 – 4.32 (m, 1H), 3.88 (s, 3H), 3.68 (q, *J* = 7.9, 7.5 Hz, 2H), 3.61 (s, 3H), 3.40 (s, 3H), 3.34 (s, 3H), 3.26 (s, 3H), 2.58 – 2.46 (m, 2H), 2.38 (t, *J* = 2.6 Hz, 1H), 2.25 – 2.13 (m, 1H), 2.05 (qt, *J* = 9.1, 6.8, 4.7 Hz, 1H), 1.71 – 1.62 (m, 6H). ^{13}C NMR (101 MHz, $CDCl_3$): δ 173.81, 173.43, 169.93, 156.19, 153.23, 144.38, 140.80, 139.62, 139.56, 139.42, 138.12, 136.94, 136.34, 133.92, 132.84, 132.66, 130.72, 129.93, 120.77, 104.63, 103.06, 102.42, 95.10, 79.25, 72.52, 52.49, 52.41, 51.81, 47.42, 38.15, 30.84, 30.49, 28.77, 22.48, 19.60, 17.59, 12.46, 12.12, 11.30. MS (MALDI): calculated for $C_{39}H_{41}N_5O_5Pd$ $[M]^+$ m/z 764.2; found m/z 764.6.

4.3 Docking analysis

Three-dimensional (3D) model of EGFR complex with erlotinib was downloaded from PDB (PDB: 1M17). The initial optimization of the ligands geometry was conducted utilizing the ORCA 5.0 softwares[54] package using the M06-2X functional (with the GRID3 integration) with the def2-TZVP basis set for all atoms. Subsequently, using the ultimately optimized structures, molecular

https://doi.org/10.26434/chemrxiv-2024-qsdbb **ORCID:** https://orcid.org/0000-0001-6015-099X Content not peer-reviewed by ChemRxiv. **License:** CC BY-NC-ND 4.0

docking was carried out, involving the calculation of the most favorable conformation of the complex and its binding energy. The computation was executed using the Autodock 4.2 program[55], with the AutoGrid program utilized for generating the docking area. The MGLTools 1.5.6 package was employed to prepare the initial data. Each docking experiment was conducted using the LGA genetic algorithm, encompassing 100 conformations with 2,500,000 calculations each. The crystal structure of the EGFR complex with erlotinib was applied (PDB: 1M17). The cluster exhibiting the most negative binding Gibbs energy was selected as the most accurate solution. The alignment of ligands was visualized using the UCSF Chimera program[56].

4.4 Photophysical measurements

All the compounds were dissolved in dH_2O + 5% DMSO (95:5, v/v) at 1 mM (stock solutions). For measuring the photophysical properties and cell studies, the stock solutions were further diluted with deionized water.

Absorption and fluorescence spectra were registered using a Synergy MX spectrophotometer-spectrofluorometer (BioTek, USA). Fluorescence was excited at 410 nm.

The molar extinction coefficient ε was determined using the following equation:

$$\varepsilon = {}^{D}/_{cl} \ ,$$

where D is the optical density; l is the path length; and c is concentration.

The fluorescence quantum yield φ1 was calculated using the equation:

$$\varphi_1 = \frac{\varphi_2 F_1 D_2}{F_2 D_1} \ ,$$

where F_1 and D_1 are the integral fluorescence intensity and the optical density of a photosensitizer being measured, φ_2 is the quantum yield of Rhodamine B (Sigma, USA) in water (0.31); F_2 and D_2 are the integral fluorescence intensity and the optical density of Rhodamine B, respectively.

The optical density was measured at 410 nm; the fluorescence was excited at the same wavelength was and detected at 550–850 nm.

4.5 Photobleaching experiments

https://doi.org/10.26434/chemrxiv-2024-qsdbb **ORCID:** https://orcid.org/0000-0001-6015-099X Content not peer-reviewed by ChemRxiv. **License:** CC BY-NC-ND 4.0

The tested conjugates were dissolved in dH_2O + 5% DMSO (95:5, v/v) at 1 mM (stock solutions). For measuring the photophysical properties, stock solutions were further diluted with deionized water.

Photobleaching measurements were carried out for 5 μM of the compounds in 96-well plates using the LED light source (655−675 nm, 32 mW/cm^2) for irradiation of the samples. Absorption spectra before and after irradiation were recorded at 450-700 nm with a Synergy MX plate reader (BioTek).

4.6 Singlet oxygen generation experiments

1,3-Diphenylisobenzofuran (DPBF) or anthracene-9,10-diylbis-methylmalonate (ADMA) was used as the singlet oxygen sensitive trap. A traps' bleaching during the photoinduced reaction was registered at every step using a Synergy MX spectrophotometer-spectrofluorometer (BioTek). The optical densities of a reaction medium containing 80 μM DPBF and 0.1 μM compound in DMSO were recorded at 420 nm before irradiation and after irradiation in doses up to 1 J/cm^2 with 0.5 J/cm^2 step. The optical densities of a reaction medium containing 250 μM ADMA and 10 μM compound in PBS were recorded at 380 nm before irradiation and after irradiation in doses up to 5 J/cm^2 with 0.5 J/cm^2 step. Irradiated using the LED a light source (655−675 nm, 32 mW/cm^2).[57]

Quantum yields of the singlet oxygen generation (Φ_Δ) were determined for the first linear stage of the DPBF or ADMA bleaching by a comparative method using the following equation:

$$\Phi_{\Delta 1} = \Phi_{\Delta 2} \frac{(D_0 - D)_1}{(D_0 - D)_2}$$

where $\Phi_{\Delta 1}$ is the quantum yield of the analyzed compound, $\Phi_{\Delta 2}$ is the quantum yield of Photodithazine® used as a reference [0.56][58], D_0 and D are the optical density at 420/380 nm before and after irradiation.

4.7 Cell line and culturing conditions

Cell lines of human epidermoid carcinoma A431 and human keratinocytes HaCat (both lines obtained from Russian Collection of Cell Cultures of Vertebrates) were cultured in Eagle's minimum essential medium (MEM) (PanEco, Russia) with 10% (v/v) fetal calf serum (HyClone)

https://doi.org/10.26434/chemrxiv-2024-qsdbb **ORCID:** https://orcid.org/0000-0001-6015-099X Content not peer-reviewed by ChemRxiv. **License:** CC BY-NC-ND 4.0

and 2 mM L-glutamine in 5% CO_2 at 37°C. At each passaging stage, the cells were treated with trypsin-ethylenediaminetetraacetic acid (EDTA) (1:1) solution (PanEco, Russia). All cells were washed with 10 mM phosphate-buffered saline (PBS).

4.8 Study of cellular uptake of the tested compounds

The cells were seeded in a 96-well plate (Corning) at the density 5×10^3 cells per well and allowed to attach overnight. Then, the medium was exchanged with fresh serum-free growth medium containing 5 μM of a tested compound (200 μL per well) and the cells were incubated for 1h, 4h, 6h and 24 h.

For analysis of intracellular localization, the cells were incubated with the tested compound at 5 μM for 24 h and then stained with the following dyes according to the manufacturer's instructions (Thermo Fisher Scientific): 0.5 μM LysoTracker Green DND-26, 0.5 μM MitoTracker Green FM, 0.5 μM ER-Tracker, 5 μM BODIPY FL C5-ceramide complexed to BSA for the Golgi apparatus, and 1X working solution CellMask Plasma Membrane Green Stain.

Cells were imaged using a laser scanning confocal microscope Axio Observer Z1 LSM 710 NLO/Duo (Carl Zeiss, Germany) equipped with C-Apochromat 63× water immersion objective lens with numerical aperture 1.2. Fluorescence of the compounds was excited at 633 nm and recorded in the range of 650−735 nm. Fluorescence of stained organelles was excited by an argon laser at 488 nm and recorded in the range of 500−550 nm.

Fluorescence intensity measurements and colocalization analysis were carried out using the ZEN 2012 program.

4.9 Cytotoxicity study

The effect of tested compounds on cell viability was estimated using the microculture tetrazoline test (MTT)[50]. Cells were seeded in 96-well plates at the density of 4×10^3 cells per well and allowed to attach overnight. The medium was then exchanged with fresh serum-free growth medium containing tested compounds in varying concentrations. After 24 h incubation, the medium was exchanged with full fresh growth medium. To estimate the photoinduced toxicity of the tested

https://doi.org/10.26434/chemrxiv-2024-qsdbb **ORCID:** https://orcid.org/0000-0001-6015-099X Content not peer-reviewed by ChemRxiv. **License:** CC BY-NC-ND 4.0

compound, we exposed the cells to light irradiation (655−675 nm, 32 mW/cm^2, 20 J/cm^2) using a LED light source[57]. Irradiated cells were then incubated for 24 h before cell viability was measured. For this, the cells were incubated with serum-free medium containing 0.5 mg/mL MTT reagent [3-(4,5-dimethyl-2-thiazolyl)-2,5-diphenyl-2H-tetrazole bromide, Alfa Aesar, U.K.] for 4 h. The formazan formed from the reduction of MTT by cell dehydrogenases was dissolved in DMSO, and the absorbance was measured at 570 nm with a Synergy MX plate reader.

The same procedure was performed for the estimation of the dark toxicity of the conjugates, except for that there was no cell exposure to LED light.

Cell viability was expressed as the ratio of the optical density of treated and untreated cells (in percentage). Three independent experiments (all in triplicate) were performed. Data analysis and calculation of half-maximal inhibition concentration IC_{50} were performed using the GraphPad Prism 6 software and a four-parameter model for the lognormal distribution.

4.10 Animal Tumor Model

Animal experiments were carried out using Balb/c Nude female mice (mass 19−23 g; 21 animals). A suspension of human epidermoid carcinoma A431 cells (3 million cells) in 10 mM PBS (100 μL, pH 7.4) was inoculated subcutaneously into the dorsal side of a right hind limb. Experiments were started 14 days after inoculation when the tumor volume reached ~0.05 cm^3. All experimental procedures were approved by the Animal Care and Use Committee of Nizhny Novgorod State University, Russia.

4.11 Pharmacokinetic Study

For fluorescent analysis of **14** and **16** in plasma blood was taken from the retro-orbital sinus before and after injection, and also after 0.25, 0.5, 1 and 4 hours after injection at a dose of 8 mg/kg. Plasma was obtained from blood by centrifugation at 12,000 rpm for 5 min and fluorescence spectra was registered using a Synergy MX spectrophotometer-spectrofluorometer (BioTek, USA). Fluorescence was excited at 410 nm.

4.12 Fluorescence whole-body imaging

https://doi.org/10.26434/chemrxiv-2024-qsdbb **ORCID:** https://orcid.org/0000-0001-6015-099X Content not peer-reviewed by ChemRxiv. **License:** CC BY-NC-ND 4.0

Accumulation and clearance of **14** and **16** in tumor and normal tissues were studied using a whole-animal fluorescence imaging system. Conjugate **14** and **16** were solubilized at 0.5 mM in water with 20% ethanol and 30% PEG2000 and injected into the tail vein at the dose of 8 mg/kg.

The fluorescence images were performed before administration of **14** and **16** and then at various time points for 24 h. Fluorescence was excited at 590 nm and recorded in the spectral band of 600−700 nm. Quantitative analysis of the captured fluorescence images was performed using ImageJ freeware. An averaged fluorescence signal was calculated in each image for two regions of interest (ROIs): the tumor area and a region of the same area positioned on the other leg (normal tissue). The contrast value was calculated as the ratio of the fluorescence signal in the tumor area to that of the normal tissue.

At 4h and 24h postinjection, mice were euthanized and the organs (brain, heart, lung, liver, spleen, kidney, stomach, intestine, muscles, skin, and tumors) were excised and weighed for *ex vivo* analysis.

Fluorescence of organs and tumor was excited at 590 nm and recorded in the spectral band of 600−700 nm. The appropriate ROIs that surround the organs were drawn using the hand, after which the software calculated the total radiant efficiency for each ROI.

Finally, organs and tumor were frozen and stored at -20ºC until further analysis.

4.13 Elemental analysis

For the biodistribution study, main organs and tumor samples were collected and weighed. Then, tissues were completely dissolved in 3-fold volume of concentrated nitric acid by heating at 80 ºC for 0.5 h. The samples were diluted 10-fold with distilled water and tubes were centrifuged at 500 g, 5 min. Concentration of porphyrazines were measured by analyzing In and Zn elements in samples using inductively coupled mass-spectrometry (NexION 2000, Perkin Elmer, USA). Background levels of elements from untreated mice tissues were subtracted from the measured concentrations. ^{115}In and ^{66}Zn isotopes were used for analysis.

4.14 PDT

https://doi.org/10.26434/chemrxiv-2024-qsdbb **ORCID:** https://orcid.org/0000-0001-6015-099X Content not peer-reviewed by ChemRxiv. **License:** CC BY-NC-ND 4.0

Three groups of animals were formed: "**16**" group (administration of **16** without PDT, n = 4); "**16 + PDT**" group (administration of **16** followed with PDT, n = 4); and control group (administration of the solvent, n = 4). Conjugate **16** was solubilized at 0.5 mM in water with 20% ethanol and 30% PEG2000 and injected into the tail vein at the dose of 10 mg/kg.

To induce a photodynamic effect, we irradiated the tumor area at 4 h after the compound was injected at a dose of 50 J/cm^2 using a LED light source (620−655 nm, power density 100 mW/ cm^2). Irradiation was carried out in 2 sessions of 4 mins 10 s with a 30 s break. The total exposure time was 8 min 20 s. After the treatment, the tumor was measured with a caliper. The tumor volume was calculated by the formula:

$V=\pi (x \cdot y \cdot z)/6$

where x, y, and z correspond to the size of the tumor node in three mutually perpendicular dimensions.

Statistical analysis was performed using two-way ANOVA with multiple group comparison by Dunnett's test.

AUTHOR INFORMATION

Corresponding authors

Vasilii F. Otvagin — Department of Organic Chemistry, Lobachevsky State University of Nizhny Novgorod, Gagarina av. 23, Nizhny Novgorod 603950, Russian Federation; orcid.org/0000-0001-6015-099X

Irina V. Balalaeva — Department of Biophysics, Lobachevsky State University of Nizhny Novgorod, Gagarina av. 23, Nizhny Novgorod 603950, Russian Federation; orcid.org/0000-0002-3245-3907

Alexey Yu. Fedorov — Department of Organic Chemistry, Lobachevsky State University of Nizhny Novgorod, Gagarina av. 23, Nizhny Novgorod 603950, Russian Federation; orcid.org/0000-0003-4889-8617; Fax: +7 831-462-32-32, E-mail: afnn@rambler.ru, afedorovnn@yandex.ru

https://doi.org/10.26434/chemrxiv-2024-qsdbb **ORCID:** https://orcid.org/0000-0001-6015-099X Content not peer-reviewed by ChemRxiv. **License:** CC BY-NC-ND 4.0

Authors

Lubov V. Krylova — Department of Biophysics, Lobachevsky State University of Nizhny Novgorod, Gagarina av. 23, Nizhny Novgorod 603950, Russian Federation.

Galina P. Gribova — Department of Organic Chemistry, Lobachevsky State University of Nizhny Novgorod, Gagarina av. 23, Nizhny Novgorod 603950, Russian Federation.

Natalia S. Kuzmina — Department of Organic Chemistry, Lobachevsky State University of Nizhny Novgorod, Gagarina av. 23, Nizhny Novgorod 603950, Russian Federation; orcid.org/0000-0001-9609-1717

Ekaterina A. Fedotova — Department of Organic Chemistry, Lobachevsky State University of Nizhny Novgorod, Gagarina av. 23, Nizhny Novgorod 603950, Russian Federation.

Ivan V. Zelepukin — Laboratory of Molecular Immunology, Shemyakin-Ovchinnikov Institute of Bioorganic Chemistry of the Russian Academy of Sciences, Moscow 117997, Russian Federation.

Alexander V. Nyuchev — Department of Organic Chemistry, Lobachevsky State University of Nizhny Novgorod, Gagarina av. 23, Nizhny Novgorod 603950, Russian Federation; orcid.org/0000-0002-0460-0543

Complete contact information is available at

Author Contributions

⊥L.V.K. and V.F.O. contributed equally to this work. All authors have given approval to the final version of the manuscript.

Notes

The authors declare no competing financial interest.

https://doi.org/10.26434/chemrxiv-2024-qsdbb **ORCID:** https://orcid.org/0000-0001-6015-099X Content not peer-reviewed by ChemRxiv. **License:** CC BY-NC-ND 4.0

ACKNOWLEDGMENT

This work was supported by the Russian Science Foundation under Grant No. 24-13-00179 https://rscf.ru/en/project/24-13-00179/ in the part of synthesis, SAR studies, and *in vitro* evaluation of the compounds. The animal studies were supported by Center of Excellence «Center of Photonics» funded by the Ministry of Science and Higher Education of the Russian Federation, contract No 075-15-2022-293.

References

(1) Li, X.; Lovell, J. F.; Yoon, J.; Chen, X. Clinical Development and Potential of Photothermal and Photodynamic Therapies for Cancer. *Nat. Rev. Clin. Oncol.* **2020**, *17* (11), 657–674. https://doi.org/10.1038/s41571-020-0410-2.

(2) Alzeibak, R.; Mishchenko, T. A.; Shilyagina, N. Y.; Balalaeva, I. V.; Vedunova, M. V.; Krysko, D. V. Targeting Immunogenic Cancer Cell Death by Photodynamic Therapy: Past, Present and Future. *J. Immunother. Cancer* **2021**, *9* (1), e001926. https://doi.org/10.1136/jitc-2020-001926.

(3) Fan, W.; Huang, P.; Chen, X. Overcoming the Achilles' Heel of Photodynamic Therapy. *Chem. Soc. Rev.* **2016**, *45* (23), 6488–6519. https://doi.org/10.1039/C6CS00616G.

(4) Sandland, J.; Boyle, R. W. Photosensitizer Antibody–Drug Conjugates: Past, Present, and Future. *Bioconjug. Chem.* **2019**, *30* (4), 975–993. https://doi.org/10.1021/acs.bioconjchem.9b00055.

(5) Yan, J.; Gao, T.; Lu, Z.; Yin, J.; Zhang, Y.; Pei, R. Aptamer-Targeted Photodynamic Platforms for Tumor Therapy. *ACS Appl. Mater. Interfaces* **2021**, *13* (24), 27749–27773. https://doi.org/10.1021/acsami.1c06818.

(6) Heukers, R.; van Bergen en Henegouwen, P. M. P.; Oliveira, S. Nanobody–Photosensitizer Conjugates for Targeted Photodynamic Therapy. *Nanomedicine* **2014**, *10* (7), 1441–1451. https://doi.org/10.1016/j.nano.2013.12.007.

(7) Li, S.; Jin, Y.; Su, Y.; Li, W.; Xing, Y.; Wang, F.; Hong, Z. Anti-HER2 Affibody-Conjugated Photosensitizer for Tumor Targeting Photodynamic Therapy. *Mol. Pharm.* **2020**, *17* (5), 1546–1557. https://doi.org/10.1021/acs.molpharmaceut.9b01247.

(8) Liu, Q.; Pang, M.; Tan, S.; Wang, J.; Chen, Q.; Wang, K.; Wu, W.; Hong, Z. Potent Peptide-Conjugated Silicon Phthalocyanines for Tumor Photodynamic Therapy. *J. Cancer* **2018**, *9* (2), 310–320. https://doi.org/10.7150/jca.22362.

(9) Mfouo-Tynga, I. S.; Dias, L. D.; Inada, N. M.; Kurachi, C. Features of Third Generation Photosensitizers Used in Anticancer Photodynamic Therapy: Review. *Photodiagnosis Photodyn. Ther.* **2021**, *34*, 102091. https://doi.org/10.1016/j.pdpdt.2020.102091.

(10) Jevševar, S.; Kusterle, M.; Kenig, M. PEGylation of Antibody Fragments for Half-Life Extension. In *Antibody Methods and Protocols*; Proetzel, G., Ebersbach, H., Eds.; Methods in Molecular Biology; Humana Press: Totowa, NJ, 2012; pp 233–246. https://doi.org/10.1007/978-1-61779-931-0_15.

(11) Grin, M.; Suvorov, N.; Ostroverkhov, P.; Pogorilyy, V.; Kirin, N.; Popov, A.; Sazonova, A.; Filonenko, E. Advantages of Combined Photodynamic Therapy in the Treatment of Oncological Diseases. *Biophys. Rev.* **2022**, *14* (4), 941–963. https://doi.org/10.1007/s12551-022-00962-6.

(12) Otvagin, V. F.; Kuzmina, N. S.; Kudriashova, E. S.; Nyuchev, A. V.; Gavryushin, A. E.; Fedorov, A. Yu. Conjugates of Porphyrinoid-Based Photosensitizers with Cytotoxic Drugs: Current Progress and Future Directions toward Selective Photodynamic Therapy. *J. Med. Chem.* **2022**, *65* (3), 1695–1734. https://doi.org/10.1021/acs.jmedchem.1c01953.

(13) Otvagin, V. F.; Kuzmina, N. S.; Krylova, L. V.; Volovetsky, A. B.; Nyuchev, A. V.; Gavryushin, A. E.; Meshkov, I. N.; Gorbunova, Y. G.; Romanenko, Y. V.; Koifman, O. I.; Balalaeva, I. V.; Fedorov, A. Y. Water-Soluble Chlorin/Arylaminoquinazoline Conjugate for Photodynamic and Targeted Therapy. *J. Med. Chem.* **2019**, *62* (24), 11182–11193. https://doi.org/10.1021/acs.jmedchem.9b01294.

https://doi.org/10.26434/chemrxiv-2024-qsdbb **ORCID:** https://orcid.org/0000-0001-6015-099X Content not peer-reviewed by ChemRxiv. **License:** CC BY-NC-ND 4.0

(14) Otvagin, V. F.; Nyuchev, A. V.; Kuzmina, N. S.; Grishin, I. D.; Gavryushin, A. E.; Romanenko, Y. V.; Koifman, O. I.; Belykh, D. V.; Peskova, N. N.; Shilyagina, N. Y. Synthesis and Biological Evaluation of New Water-Soluble Photoactive Chlorin Conjugate for Targeted Delivery. *Eur. J. Med. Chem.* **2018**, *144*, 740–750. https://doi.org/10.1016/j.ejmech.2017.12.062.
(15) Nyuchev, A. V.; Otvagin, V. F.; Gavryushin, A. E.; Romanenko, Y. I.; Koifman, O. I.; Belykh, D. V.; Schmalz, H.-G.; Fedorov, A. Y. Synthesis of Chlorin–(Arylamino)Quinazoline Hybrids as Models for Multifunctional Drug Development. *Synthesis* **2015**, *47* (23), 3717–3726. https://doi.org/10.1055/s-0034-1378876.
(16) Otvagin, V. F.; Krylova, L. V.; Peskova, N. N.; Kuzmina, N. S.; Fedotova, E. A.; Nyuchev, A. V.; Romanenko, Y. V.; Koifman, O. I.; Vatsadze, S. Z.; Schmalz, H.-G.; Balalaeva, I. V.; Fedorov, A. Y. A First-in-Class β-Glucuronidase Responsive Conjugate for Selective Dual Targeted and Photodynamic Therapy of Bladder Cancer. *Eur. J. Med. Chem.* **2024**, *269*, 116283. https://doi.org/10.1016/j.ejmech.2024.116283.
(17) Wang, H.; Lai, Y.; Li, D.; Karges, J.; Zhang, P.; Huang, H. Self-Assembly of Erlotinib-Platinum(II) Complexes for Epidermal Growth Factor Receptor-Targeted Photodynamic Therapy. *J. Med. Chem.* **2024**, *67* (2), 1336–1346. https://doi.org/10.1021/acs.jmedchem.3c01889.
(18) Gül, E. Y.; Karataş, E. A.; Doğan, H. A.; Karataş, Ö. F.; Çoşut, B.; Eçik, E. T. Erlotinib-Modified BODIPY Photosensitizers for Targeted Photodynamic Therapy. *ChemMedChem* **2023**, *18* (2), e202200439. https://doi.org/10.1002/cmdc.202200439.
(19) Chen, J.-J.; Huang, Y.-Z.; Song, M.-R.; Zhang, Z.-H.; Xue, J.-P. Silicon Phthalocyanines Axially Disubstituted with Erlotinib toward Small-Molecular-Target-Based Photodynamic Therapy. *ChemMedChem* **2017**, *12* (18), 1504–1511. https://doi.org/10.1002/cmdc.201700384.
(20) Cheruku, R. R.; Cacaccio, J.; Durrani, F. A.; Tabaczynski, W. A.; Watson, R.; Siters, K.; Missert, J. R.; Tracy, E. C.; Dukh, M.; Guru, K.; Koya, R. C.; Kalinski, P.; Baumann, H.; Pandey, R. K. Synthesis, Tumor Specificity, and Photosensitizing Efficacy of Erlotinib-Conjugated Chlorins and Bacteriochlorins: Identification of a Highly Effective Candidate for Photodynamic Therapy of Cancer. *J. Med. Chem.* **2021**, *64* (1), 741–767. https://doi.org/10.1021/acs.jmedchem.0c01735.
(21) Bortnevskaya, Y. S.; Shiryaev, N. A.; Zakharov, N. S.; Kitoroage, O. O.; Gradova, M. A.; Karpechenko, N. Y.; Novikov, A. S.; Nikolskaya, E. D.; Mollaeva, M. R.; Yabbarov, N. G.; Bragina, N. A.; Zhdanova, K. A. Synthesis and Biological Properties of EGFR-Targeted Photosensitizer Based on Cationic Porphyrin. *Pharmaceutics* **2023**, *15* (4), 1284. https://doi.org/10.3390/pharmaceutics15041284.
(22) Zhao, X.; Huang, Y.; Yuan, G.; Zuo, K.; Huang, Y.; Chen, J.; Li, J.; Xue, J. A Novel Tumor and Mitochondria Dual-Targeted Photosensitizer Showing Ultra-Efficient Photodynamic Anticancer Activities. *Chem. Commun.* **2019**, *55* (6), 866–869. https://doi.org/10.1039/C8CC09456J.
(23) Xiao, M.; Fan, J.; Li, M.; Xu, F.; Zhao, X.; Xi, D.; Ma, H.; Li, Y.; Du, J.; Sun, W.; Peng, X. A Photosensitizer-Inhibitor Conjugate for Photodynamic Therapy with Simultaneous Inhibition of Treatment Escape Pathways. *Biomaterials* **2020**, *257*, 120262. https://doi.org/10.1016/j.biomaterials.2020.120262.
(24) Wei, G.; Huang, L.; Jiang, Y.; Shen, Y.; Huang, Z.; Huang, Y.; Sun, X.; Zhao, C. Lenvatinib-Zinc Phthalocyanine Conjugates as Potential Agents for Enhancing Synergistic Therapy of Multidrug-Resistant Cancer by Glutathione Depletion. *Eur. J. Med. Chem.* **2019**, *169*, 53–64. https://doi.org/10.1016/j.ejmech.2019.02.065.
(25) Huang, L.; Wei, G.; Sun, X.; Jiang, Y.; Huang, Z.; Huang, Y.; Shen, Y.; Xu, X.; Liao, Y.; Zhao, C. A Tumor-Targeted Ganetespib-Zinc Phthalocyanine Conjugate for Synergistic Chemo-Photodynamic Therapy. *Eur. J. Med. Chem.* **2018**, *151*, 294–303. https://doi.org/10.1016/j.ejmech.2018.03.077.
(26) Sigismund, S.; Avanzato, D.; Lanzetti, L. Emerging functions of the EGFR in cancer. *Mol. Oncol.* **2018**, *12* (1), 3–20. https://doi.org/10.1002/1878-0261.12155.
(27) Ulfo, L.; Costantini, P. E.; Di Giosia, M.; Danielli, A.; Calvaresi, M. EGFR-Targeted Photodynamic Therapy. *Pharmaceutics* **2022**, *14* (2), 241. https://doi.org/10.3390/pharmaceutics14020241.
(28) Fallahi, P.; Di Bari, F.; Ferrari, S. M.; Spisni, R.; Materazzi, G.; Miccoli, P.; Benvenga, S.; Antonelli, A. Selective use of vandetanib in the treatment of thyroid cancer. *Drug Des. Devel. Ther.* **2015**, *9*, 3459– 3470. https://doi.org/10.2147/DDDT.S72495.
(29) Kwiatkowski, S.; Knap, B.; Przystupski, D.; Saczko, J.; Kędzierska, E.; Knap-Czop, K.; Kotlińska, J.; Michel, O.; Kotowski, K.; Kulbacka, J. Photodynamic Therapy – Mechanisms, Photosensitizers and Combinations. *Biomed. Pharmacother.* **2018**, *106*, 1098–1107. https://doi.org/10.1016/j.biopha.2018.07.049.

https://doi.org/10.26434/chemrxiv-2024-qsdbb **ORCID:** https://orcid.org/0000-0001-6015-099X Content not peer-reviewed by ChemRxiv. **License:** CC BY-NC-ND 4.0

(30) Sun, Y.; Geng, X.; Wang, Y.; Su, X.; Han, R.; Wang, J.; Li, X.; Wang, P.; Zhang, K.; Wang, X. Highly Efficient Water-Soluble Photosensitizer Based on Chlorin: Synthesis, Characterization, and Evaluation for Photodynamic Therapy. *ACS Pharmacol. Transl. Sci.* **2021**, *4* (2), 802–812. https://doi.org/10.1021/acsptsci.1c00004.
(31) Gradova, M. A.; Gradov, O. V.; Lobanov, A. V.; Bychkova, A. V.; Nikolskaya, E. D.; Yabbarov, N. G.; Mollaeva, M. R.; Egorov, A. E.; Kostyukov, A. A.; Kuzmin, V. A.; Khudyaeva, I. S.; Belykh, D. V. Characterization of a Novel Amphiphilic Cationic Chlorin Photosensitizer for Photodynamic Applications. *Int. J. Mol. Sci.* **2023**, *24* (1), 345. https://doi.org/10.3390/ijms24010345.
(32) Kollar, J.; Machacek, M.; Halaskova, M.; Lenco, J.; Kucera, R.; Demuth, J.; Rohlickova, M.; Hasonova, K.; Miletin, M.; Novakova, V.; Zimcik, P. Cationic versus anionic phthalocyanines for photodynamic therapy: what a difference the charge makes. *J. Med. Chem.* **2020**, *63* (14), 7616–7632. https://doi.org/10.1021/acs.jmedchem.0c00481.
(33) Jensen, T. J.; Vicente, M. G. H.; Luguya, R.; Norton, J.; Fronczek, F. R.; Smith, K. M. Effect of Overall Charge and Charge Distribution on Cellular Uptake, Distribution and Phototoxicity of Cationic Porphyrins in HEp2 Cells. *J. Photochem. Photobiol. B* **2010**, *100* (2), 100–111. https://doi.org/10.1016/j.jphotobiol.2010.05.007.
(34) Hirohara, S.; Kawasaki, Y.; Funasako, R.; Yasui, N.; Totani, M.; Alitomo, H.; Yuasa, J.; Kawai, T.; Oka, C.; Kawaichi, M.; Obata, M.; Tanihara, M. Sugar and heavy atom effects of glycoconjugated chlorin palladium complex on photocytotoxicity. *Bioconjug. Chem.* **2012**, *23* (9), 1881–1890. https://doi.org/10.1021/bc300223j.
(35) De Simone, B. C.; Mazzone, G.; Russo, N.; Sicilia, E.; Toscano, M. Metal Atom Effect on the Photophysical Properties of Mg(II), Zn(II), Cd(II), and Pd(II) Tetraphenylporphyrin Complexes Proposed as Possible Drugs in Photodynamic Therapy. *Molecules* **2017**, *22* (7), 1093. https://doi.org/10.3390/molecules22071093.
(36) Engelmann, F. M.; Mayer, I.; Gabrielli, D. S.; Toma, H. E.; Kowaltowski, A. J.; Araki, K.; Baptista, M. S. Interaction of cationic meso-porphyrins with liposomes, mitochondria and erythrocytes. *J. Bioenerg. Biomembr.* **2007**, *39*, 175–185. https://doi.org/10.1007/s10863-007-9075-0.
(37) Abouzid, K.; Shouman, S. Design, Synthesis and in Vitro Antitumor Activity of 4-Aminoquinoline and 4-Aminoquinazoline Derivatives Targeting EGFR Tyrosine Kinase. *Bioorg. Med. Chem.* **2008**, *16* (16), 7543–7551. https://doi.org/10.1016/j.bmc.2008.07.038.
(38) Belykh, D. V.; Tarabukina, I. S.; Gruzdev, I. V.; Kodess, M. I.; Kutchin, A. V. Aminomethylation of Chlorophyll a Derivatives Using Bis(N,N-Dimethylamino)Methane. *J. Porphyr. Phthalocyanines* **2009**, *13* (08n09), 949–956. https://doi.org/10.1142/S1088424609001133.
(39) Kustov, A. V.; Kustova, T. V.; Belykh, D. V.; Khudyaeva, I. S.; Berezin, D. B. Synthesis and Investigation of Novel Chlorin Sensitizers Containing the Myristic Acid Residue for Antimicrobial Photodynamic Therapy. *Dyes Pigments* **2020**, *173*, 107948. https://doi.org/10.1016/j.dyepig.2019.107948.
(40) Rychikhina, E.; Ivanova, S. S.; Romanenko, Y. V.; Koifman, O. I.; Stuzhin, P. A. Indium Complexes of Chlorin E6 Trimethyl Ester and Methylpyropheophorbide a: Synthesis and Photophysical Characterization. *Polyhedron* **2022**, *217*, 115743. https://doi.org/10.1016/j.poly.2022.115743.
(41) Yoon, I.; Park, H. S.; Cui, B. C.; Li, J. Z.; Kim, J. H.; Lkhagvadulam, B.; Shim, Y. K. Photodynamic and Antioxidant Activities of Divalent Transition Metal Complexes of Methyl Pheophorbide-a. *Bull. Korean Chem. Soc.* **2011**, *32* (8), 2981–2987. https://doi.org/10.5012/bkcs.2011.32.8.2981.
(42) Borisov, S. M.; Papkovsky, D. B.; Ponomarev, G. V.; DeToma, A. S.; Saf, R.; Klimant, I. Photophysical Properties of the New Phosphorescent Platinum(II) and Palladium(II) Complexes of Benzoporphyrins and Chlorins. *J. Photochem. Photobiol. Chem.* **2009**, *206* (1), 87–92. https://doi.org/10.1016/j.jphotochem.2009.05.018.
(43) Kitamura, S.; Maeda, T.; Yanagi, T. Vandetanib Inhibits Cell Growth in EGFR-Expressing Cutaneous Squamous Cell Carcinoma. *Biochem. Biophys. Res. Commun.* **2020**, *531* (3), 396–401. https://doi.org/10.1016/j.bbrc.2020.07.111.
(44) Keyal, U.; Bhatta, A. K.; Zhang, G.; Wang, X. L. Present and Future Perspectives of Photodynamic Therapy for Cutaneous Squamous Cell Carcinoma. *J. Am. Acad. Dermatol.* **2019**, *80* (3), 765–773. https://doi.org/10.1016/j.jaad.2018.10.042.
(45) Figliola, C.; Anton, H.; Sutter, C.; Chériaux, C.; Sutter, A.; Mazan, V.; Elhabiri, M.; Didier, P.; Jacquemin, D.; Ulrich, G. Lysosomes Targeting pH Activable Imaging-Guided Photodynamic Agents. *ChemBioChem*. **2023**, *24* (12), e202300139. https://doi.org/10.1002/cbic.202300139.

https://doi.org/10.26434/chemrxiv-2024-qsdbb **ORCID:** https://orcid.org/0000-0001-6015-099X Content not peer-reviewed by ChemRxiv. **License:** CC BY-NC-ND 4.0

(46) Kessel, D.; Oleinick, N. L. Cell Death Pathways Associated with Photodynamic Therapy: An Update. *Photochem. Photobiol.* **2018**, *94* (2), 213–218. https://doi.org/10.1111/php.12857.
(47) Arnott, J.A; Planey, S.L. The influence of lipophilicity in drug discovery and design. *Expert Opin. Drug Discov.* **2012**, *7 (10)*, 863. https://doi.org/10.1517/17460441.2012.714363.
(48) Liu, B.; Qi, W.; Tian, L.; Li, Z.; Miao, G.; An, W.; Liu, D.; Lin, J.; Zhang, X.; Wu, W. In Vivo Biodistribution and Toxicity of Highly Soluble PEG-Coated Boron Nitride in Mice. *Nanoscale Res. Lett.* **2015**, *10*, 478. https://doi.org/10.1186/s11671-015-1172-0.
(49) Simões, J. C. S.; Sarpaki, S.; Papadimitroulas, P.; Therrien, B.; Loudos, G. Conjugated Photosensitizers for Imaging and PDT in Cancer Research. *J. Med. Chem.* **2020**, *63* (23), 14119–14150. https://doi.org/10.1021/acs.jmedchem.0c00047.
(50) Mosmann, T. Rapid Colorimetric Assay for Cellular Growth and Survival: Application to Proliferation and Cytotoxicity Assays. *J. Immunol. Methods* **1983**, *65* (1–2), 55–63. https://doi.org/10.1016/0022-1759(83)90303-4.

https://doi.org/10.26434/chemrxiv-2024-qsdbb **ORCID:** https://orcid.org/0000-0001-6015-099X Content not peer-reviewed by ChemRxiv. **License:** CC BY-NC-ND 4.0